# THERMAL ANALYSIS OF TRUNCATED AEROSPIKE NOZZLE USING CFD

PROJECT REPORT

submitted by

**GAYATHRI PRASAD T (TKM17ME054)**

**J J JAYASOORYA (TKM17ME066)**

**ROHIN K RAJEEV (TKM17ME110)**

**SAMRIN FATHIMA(TKM17ME114)**

*the APJ Abdul Kalam Technological University*
*in partial fulfillment of the requirements for the award of Bachelor of Technology degree in Mechanical Engineering*


**Department of Mechanical Engineering**

T K M College of Engineering, Kollam
July 2021

**DEPARTMENT OF MECHANICAL ENGINEERING**
**T K M COLLEGE OF ENGINEERING, KOLLAM**

# CERTIFICATE

Certified that this report entitled '*Thermal analysis of truncated aerospike nozzle'* is the interim report of project presented by **GAYATHRI PRASAD T (TKM17ME054), J J JAYASOORYA (TKM17ME066), ROHIN K RAJEEV (TKM17ME110), SAMRIN FATHIMA (TKM17ME114)** during 2020-2021 in partial fulfillment of the requirements for the award of the Degree of Bachelor of Technology in Mechanical Engineering of the *APJ Abdul Kalam Technological University.*

Dr. K E Reby Roy
Associate Professor
Dept. of Mechanical Engineering
T K M College of Engineering, Kollam

Dr. Mohammed Sajid N.K
Head of the Department
Dept. of Mechanical Engineering
T K M College of Engineering, Kollam

# DECLARATION

We, Gayathri Prasad T, J J Jayasoorya, Rohin K Rajeev and Samrin Fathima hereby declare that this project report entitled Thermal Analysis of Truncated Aerospike Nozzle using CFD is our bonafide work carried out under the supervision of Dr. K E Reby Roy, Associate Professor of Department of Mechanical Engineering, T K M College of Engineering, Kollam. We declare that to the best of our knowledge, the work reported herein does not form part of any other project report or dissertation on the basis of which a degree or award was conferred on an earlier occasion to any other candidate. The content of this report is not being presented by any other student to this or any other University for the award of a degree.

Signature :

1) Gayathri Prasad T (TKM17ME054)

2) J J Jayasoorya (TKM17ME066)

3) Rohin K Rajeev (TKM17ME110)

4) Samrin Fathima (TKM17ME114)

Signature(s):

Name of Guide(s): Dr. K E Reby Roy

Countersigned with Name: Dr. Mohammed Sajid N.K.

Head, Department of Mechanical Engineering

T K M College of Engineering, Kollam. Date:…../07/2021

# ACKNOWLEDGEMENTS

We take this opportunity to express our deep sense of gratitude to all who helped us to complete our project successfully.

We are deeply indebted to our guide **Dr. K E Reby Roy**, Associate Professor of the Department of Mechanical Engineering for his excellent guidance, support and valuable comments. We express our sincere gratitude to **Dr. Mohammed Sajid N.K**, Head of the Department, Department of Mechanical Engineering, for his support and cooperation.

We thank our parents, friends, near and dear ones who directly or indirectly contributed to the successful completion of our project. Finally, we thank the Almighty for his blessings without which this would not have been successful.

Place: Kollam

Date :

Rohin K Rajeev

Gayathri Prasad T

Samrin Fathima

J J Jayasoorya

# ABSTRACT

Increased interest in the launch of satellites/spacecraft has driven the development of alternative, more efficient rocket nozzles. The aerospike nozzle is designed to achieve thrust at varying altitudes employing a unique geometrical design. This project involves the design and thermal analysis of a truncated aerospike nozzle using ANSYS Fluent. For a single-stage-to-orbit (SSTO) vehicle, some form of altitude compensation in the nozzle is a must. An SSTO vehicle relies on a single propulsion system that operates from sea level to orbit. The aerospike engine is proved to have a potential use with an SSTO Reusable Launch vehicle (RLV) because of its built-in altitude compensation features and the beneficial manner in which it integrates with the vehicle. The concept of aerospikes is the opposite of a bell nozzle which expands the flow away from the axis along diverging nozzle walls. In a standard bell nozzle, flow expansion continues regardless of the ambient pressure. The flow can continue to over-expand until it separates from the nozzle walls, which may affect the nozzle performance; hence the need for aerospikes arises. Although its design makes it superior in comparison with the conventional bell nozzles, a significant predicament in the realisation of these aerospikes is its performance under thermal conditions.

This project focuses on the study and research on the thermal effects of a truncated aerospike nozzle, a variant of linear aerospike. The effect of hot flow gases on the nozzle body and their influence on the surrounding atmosphere are discussed and analysed in this project.



**Keywords**: Aerospike nozzle, single-stage-to-orbit (SSTO), altitude compensation, thermal effects

# CONTENT

# LIST OF FIGURES

# LIST OF TABLES

# CHAPTER 1: INTRODUCTION

The reduction of Earth-to-orbit launch costs in conjunction with an increase in launcher reliability and operational efficiency are the key demands on future space transportation systems, like single-stage-to-orbit vehicles (SSTO). The future of advanced rocket nozzle is already on the go, as seen in the rocket engine with a linear plug nozzle is foreseen as the propulsion system for the Lockheed Martin lifting body RLV (Reusable Launch Vehicle) X-33 concept. The substantial cost of transporting payload into orbit has created the demand for a reusable, single-stage launch system. It has been estimated that a reusable single-stage launch system can reduce the cost per kilogram to orbit by order of magnitude.

A convergent-divergent nozzle (De Laval Nozzle) is the most commonly used type, despite the limitation arising from its fixed geometry characteristics. It was designed by Giovanni Battista Venturi, which was generally known as Venturi tubes that were used to experiment with the effects in fluid pressure reduction while flowing through chokes (Venturi effect). German engineer and inventor Ernst Körting supposedly switched to a converging-diverging nozzle in his steam jet pumps by 1878 after using convergent nozzles, but these nozzles remained a company secret. Later, a new design of the same nozzle was implemented on an impulse turbine by Swedish engineer Gustav De Laval in 1988. Laval's Convergent-Divergent nozzle was first applied in a rocket engine by Robert Goddard. Most modern rocket engines that employ hot gas combustion use de Laval nozzles.

Propulsion systems fitted with conventional convergent-divergent nozzles which operate from sea level to the vacuum conditions (Space Shuttle Main Engine, Vulcan) are currently subject to efficiency losses of up to 15%. The fixed area ratio design employed in these nozzles produces efficiency losses by forcing the exhaust pressure at the nozzle exit plane to remain constant. As the receiver or local atmospheric pressure is a function of altitude, optimal efficiency is restricted to a single altitude for a fixed nozzle, with pressure losses incurred at all other altitudes.

To increase the feasibility of single-stage launch systems, techniques to compensate for the variation in atmospheric conditions are required. The plug and truncated plug (aerospike) nozzle have arguably received the most attention out of all altitude adaptive nozzle concepts

irrespective of the significant base drag, increased heat flux, and variation in thrust levels at transonic velocities.

The high-temperature mix of gas coming out of the combustion chamber is directed towards one direction that flows along the walls of the aerospike due to the constant influence of ambient pressure even when there are considerable variations in its values as altitude increases. The presence of a viscous separated wake and free expansion surfaces within the nozzle flowfield enables a truncated plug nozzle to adjust to ambient conditions. This reduces overexpansion losses at low altitudes and minimizes under expansion losses at high altitudes. The truncation of the central plug body, which is an advantage because of the enormous length and high structural mass of the well-contoured central body, results in a different flow and performance behaviour than the full-length plug nozzle. Truncated plug exhaust nozzles may be integrated into any air-breathing or rocket engine and have the added advantage of reduced size and weight. At low chamber values to ambient pressure ratio, the separated flow region is "open" (i.e., sensitive to ambient conditions) and unsteady. Due to the relatively high ambient pressure, the external boundary is inclined toward the nozzle axis. The combined effects of the "open wake" and the position of the external boundary result in a low overall nozzle area ratio during low altitude operation as the chamber to ambient pressure ratio increases, the jet mixing region (the shear layer between nozzle exhaust flow and separated flow region) moves toward the nozzle axis. The external boundary moves away from the nozzle axis. This produces a continuously increasing effective nozzle area ratio as the vehicle altitude increases. During the open wake regime of operation, the base pressure is essentially equal to the ambient pressure. At some point in the trajectory, when the chamber to ambient pressure ratio has increased sufficiently, the wake "closes," and the separated base region is no longer sensitive to ambient conditions. The structure of the nozzle flowfield (including the base pressure) for closed wake operation is of particular interest since this represents design operating conditions. Also, for most nozzles of practical interest, the wake would be closed for a significant portion of the flight. Nozzle area ratio adjustment still occurs during closed wake operation since the external boundary moves away from the nozzle axis as the ambient pressure decreases. This continual adjustment of area ratio with altitude is the reason for the designation altitude compensating nozzle.

The performance of aerospike on engines used in rockets began around the 1960s. The Los Angeles-based American rocket design company Rocketdyne conducted a series of tests on its well-known J2 engines, which showed the same thrust levels as the conventional engines they were based on. The XRS-2200 was an experimental linear aerospike engine developed in the mid-1990, from which the RS-2200 was developed that was used by VentureStar for NASA' X-22 project. The program was eventually stopped in early 2001 due to insufficient funding from the Space Launch Initiative.

Though the aerospike nozzle has many advantages such as uniform load distribution, simple gas dynamic configuration, and flexible structure combinations, such nozzle faces many hurdles due to its aerodynamic and structural design considerations. The altitude compensation capability of circular and linear plug nozzles for higher ambient pressures is indisputable. For high-area-ratio nozzles with relatively short lengths, plug nozzles perform better than conventional bell nozzles. In addition to having excellent capabilities for altitude compensation, plug nozzles have additional advantages, including ease in vehicle and engine integration. To contain the extreme heating loads on the annular throat and nozzle, a combination of regenerative cooling, film cooling, and dump cooling using hydrogen must be employed. Performance analysis on cold flow conditions has been done and studied so far, and that on the hot flow conditions are yet to be conducted.

Aerospikes with truncations of 20,40, and 60% were considered in previously published papers to study flow separation and its effect on the aerospike performance. Flow separation due to restricted shock separation was found in all truncated nozzles except for 20% due to its reduced nozzle size. This reduction of length causes a reduction in thrust. However, the flow changes from the open-wake region to the closed-wake region at a lower NPR are desirable for practical application.

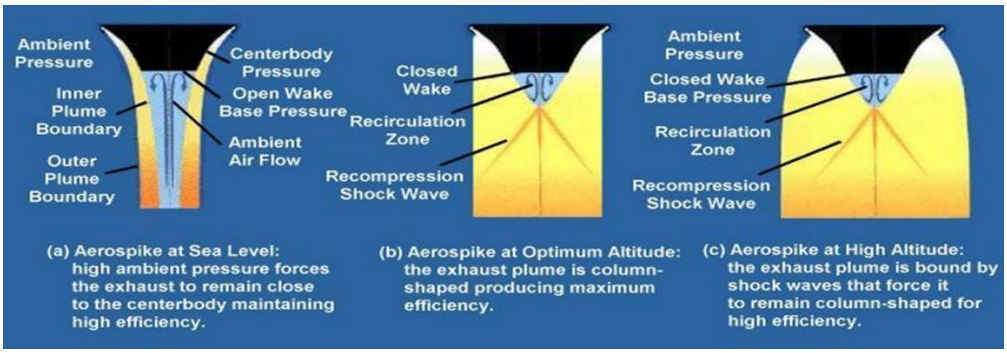

# CHAPTER 2: LITERATURE REVIEW

It was Griffith in 1954 that first addressed aerospike nozzles as an option for altitude compensation, and Rocketdyne further promoted this. Sule and Mueller, in 1973, conducted a study on the base pressure characteristics of an annular truncated plug nozzle. The study showed that open-wake and closed-wake regions could be identified from base pressure characteristics. During the open wake mode, the base pressure kept decreasing, and finally, when the wake closed, the base pressure became constant and remained unchanged upon the further decrease in backpressure. This study helped in understanding the effects of base pressure on the performance of the nozzle. The potential of an aerospike nozzle to replace the conventional aerospike nozzle was realized by many researchers in the late 1970s. The works of Humphreys et al. in 1971 and Migdal et al. in 1972 on annular plug nozzles helped in developing the branches for linear and conical aerospike nozzle.

Verma et al., in 2009, conducted an experimental investigation to study the performance and base pressure characteristics of a Mach 2.0 annular conical aerospike nozzle (full length and 40% truncation) with and without freestream flow. The effect of cowl length, plug length, and plug contour variation on the nozzle performance and base pressure characteristics were also studied. It was observed that for no freestream conditions, the performance of a full-length conical aerospike nozzle differs from the ideal case at almost all Nozzle Pressure Ratio (NPR) tested. Also, a reduction in the cowl length reduces the performance of the nozzle. In the presence of freestream conditions, the performance of the tested configurations further drops at the highest NPR. Further, it was understood that in order to avoid flow separation at low NPR, it is preferred to use shorter plug nozzles so that they can switch to a closed-wake regime at lower altitudes.

Verma and Viji, in 2011, conducted an experimental investigation to study the effect of freestream flow and cowl-length variation on upstream flow interference effects and the base wake-closure nozzle pressure ratio. Therefore, the main objective of the investigation was to correlate the variations in base pressure with changes in the upstream flow interference on the afterbody and to those on the plug surface as a function of nozzle pressure ratio and cowl-length variation. The results obtained from the study were that at lower freestream Mach numbers, the upstream flow interference seems to be insensitive to the exhaust flow NPR.

However, for M=1.64, the upstream influence is sensitive and decreases with an increase in NPR. Increasing the cowl length further reduces the upstream flow interference effects significantly in each test case. Also, in the presence of freestream, the reduced momentum thrust from the inner nozzle at similar NPR delays the movement of overexpansion shock on the plug surface for NPR>4. In the case of a truncated plug, this delays the onset of base-wake closure and increases the base-wake closure NPR with increasing freestream Mach number. For this particular study the freestream Mach number was chosen to be 1.57. This is a favourable condition from the viewpoint of altitude compensation effects. Increasing the cowl length also helps to increase the base pressure thrust contribution at all operating conditions.

In 2015, He Miaosheng, Qin Lizi, and Liu Yu conducted a detailed numerical study on the flow separation behaviour with nozzle pressure ratio (NPR) at various altitudes. The study provides an insightful understanding of the shock physics and characteristics of shock/boundary-layer interactions at various operating conditions, from highly over-expanded conditions to the designed point of the nozzle. Additionally, the gas density effect on the flow characteristics was studied. P.P Nair et al., in 2017conducted a detailed analysis of flow-through 20% and 40% aerospike nozzle using computational fluid dynamics technique. The study gave a brief overview of the ill effects of flow separation at low NPR, and in order to reduce this effect, truncated plug nozzles are suggested in which there is no reattachment of flow due to shorter length. Ito et al. performed a computational study on axisymmetric contoured plug nozzle and 25 deg half-angle conical plug nozzle. The study revealed that the performance of the contoured plug nozzle was 5–6% higher than the conical plug nozzle, and the base thrust at higher altitudes could compensate for the thrust due to truncation.

P.P Nair et al., in 2019, published a paper titled Study of Conical Aerospike Nozzles with Base-Bleed and Freestream Effects, which gives an overview on flow characteristics within conical aerospike nozzles with different levels of truncation and flow conditions. They conducted a computational fluid dynamics simulation on a 15 deg half-angle annular conical spike nozzle with different nozzle lengths (20% and 40%) at different NPRs. The paper's findings suggest that the flow separation due to restricted shock separation at a low NPR was absent for 20% aerospike nozzle. The performance loss due to trimming could be compensated by providing base bleed.

When base bleeding was introduced from the outer portion of the base, the performance increased compared to the base bleeding introduced from the center of the base.

J. Harroun et al. conducted a comparative study between an aerospike nozzle and a nozzle-less geometry to determine the performance gain in a rotating detonation engine (RDE). The journal summarizes the comparison study between RDE's with and without aerospikes. The aerospike nozzle improved the engine's specific impulse by up to 16% compared to the nozzle-less geometry.

# CHAPTER 3: OBJECTIVES & PROBLEM STATEMENT

## 3.1 OBJECTIVES

In the analysis of an aerospike nozzle, the focus so far has always been on the flow performance and its characteristics. Results and analysis based on thermal effects are not seen as much as that of the flow characteristics. Understanding the consequences of a high-temperature exhaust on the nozzle body and its surrounding is crucial for its operation. An aerospike nozzle with its unique geometrical features is significantly influenced by temperature as the main spike body is fully engulfed in the hot gas flue of the rocket exhaust and is thus susceptible to rapid ablation, weakening and damage, making it unusable after a single flight, even restricting the length of time it may operate during that flight. The domain of temperature influences can also be seen during the interaction of the surrounding atmosphere with hot flue gases, where changes in freestream conditions can be observed.

After an extensive literature review on topics associated with aerospikes, we concluded that deducing a thermal study based on the observations found on papers with results of flow characteristics was the next step in further understanding the concepts of aerospike. The values of flow characteristics that we applied in temperature analysis, from the paper by Prashant et al., 2017, were as follows: Truncation - 20%, Freestream Mach Number-2.57, NPRs - 2.87, 3.8 and 6.5.

## 3.2 PROBLEM STATEMENT

- To conduct a numerical study on the aerodynamic behaviour and performance at NPRs 2.57,3.8 and 6.5, of a 15º half-angle annular conical aerospike nozzle, with 20% truncation, inside a wind tunnel of dimensions 4.5m x 0.5m.
- To investigate and identify the regions where heat flux distribution is maximum to prevent material damage due to thermal effects.
- To determine the extent to which the exhaust gas temperature approaches the ambient temperature along the domain.
- To understand the variation in heat distribution values when a cooling channel of width 1.98mm is provided on the exterior surface of the nozzle body at different NPRs.

# CHAPTER 4: METHODOLOGY

## 4.1 GOVERNING EQUATION

The numerical analysis of the proposed 20% truncated conical aerospike is carried out using the Ansys fluent software. For that a 2D axisymmetric geometrical model of the aerospike nozzle is created and the study is carried out by solving the steady, Reynolds-averaged Navier–Stokes equations are solved along with the two-equation Menter shear stress transport (SST) k – ω turbulence model. The flow inside the nozzle is assumed to be ideal and thus the above system of equations is closed with the ideal gas equation of state. the viscosity of the flow was defined by Sutherland's law with three coefficients. The following governing equations are used for the numerical simulation:

- For 2D axisymmetric geometry the continuity equation is given by:

$$\frac{\partial \rho}{\partial t} + \frac{\partial}{\partial x}(\rho v_X) + \frac{\partial}{\partial r}(\rho v_r) + \frac{\rho v_r}{r} = 0 \qquad (4.1)$$

where x is the axial coordinate, r is the radial coordinate, $v_x$ is the axial velocity, and $v_r$ is the radial velocity.

- Momentum equation:

$$\nabla \cdot (\rho v v) = -\nabla p + \nabla \cdot \mu \left[ (\nabla v) - \tfrac{2}{3} \nabla \cdot v I \right] \qquad (4.2)$$

- Energy equation:

$$\nabla \cdot v(\rho E + p) = \nabla \cdot \left[ \left( k_t + \frac{C_p \mu_t}{p r_t} \right) \nabla T + \mu_{eff} \left[ (\nabla \cdot v) - \frac{2}{3} \nabla \cdot v I \right] \cdot v \right] \qquad (4.3)$$

where p is the static pressure, ρ is the density, μ is the molecular viscosity, I is the unit tensor, $k_T$ is the thermal conductivity, E is the total energy, and T is the temperature.

## 4.2 TURBULENCE MODEL

The Menter's two-equation shear stress transport (SST) k − ω model is used for the computational analysis. This model was selected due to its robustness, economy, and reasonable accuracy for a wide range turbulent flow. The SST k – ω model also shows good behaviour in adverse pressure gradients and separating flows. It can also be seen from the studies of Perigo and Qin, Kurbatskii and Montanari, Xiao et al., Allamaprabhu et al., and

Miaosheng et al. that the menter's SST k – ω model provided a better prediction of flow characteristics when the flow separation is caused by shock. It is based on the model equations of turbulent kinetic energy k and specific rate of dissipation ω as given in the following:

$$\frac{\partial}{\partial X_i}\left(\rho k u_{i)} = \frac{\partial}{\partial X_j}(\Gamma_k \frac{\partial k}{\partial X_j}\right) + G_k - Y_K \tag{4.4}$$

$$\frac{\partial}{\partial X_i}(\rho w u_i) = \frac{\partial}{\partial x_j}\left(\Gamma_\omega \frac{\partial \omega}{\partial X_j}\right) + G_\omega - Y_\omega + D_\omega \tag{4.5}$$

In these equations, $G_k$ represents the generation of k due to mean velocity gradients, $G_\omega$ represents the generation of ω, and $\Gamma_k$ and $\Gamma_\omega$ represent the effective diffusivity of k and ω, respectively. $Y_{ks}$ and $Y_\omega$ represent the dissipation of k and ω due to turbulence, and $D_\omega$ represents the cross-diffusion term.

## 4.3 GEOMETRY DETAILS AND COMPUTATIONAL DOMAIN

A truncated conical aerospike nozzle with 15 deg half-angle is used for the computational analysis in this work and its geometrical dimensions are shown in Fig 1 and fig 2. Fig 1 shows a conical full spike nozzle, the length of a full spike nozzle from the throat is 59.71mm and it will be reduced to 11.94 in case of a 20% truncated nozzle. The length of the cowl l, measured from the cowl tip to the throat, was 9.0 mm, and the area ratio of the inner nozzle $\varepsilon_i$= 1.19. The exit nozzle radius $r_e$ was fixed as 25 mm. The annular gap at the throat $h_t$ is 9 mm.

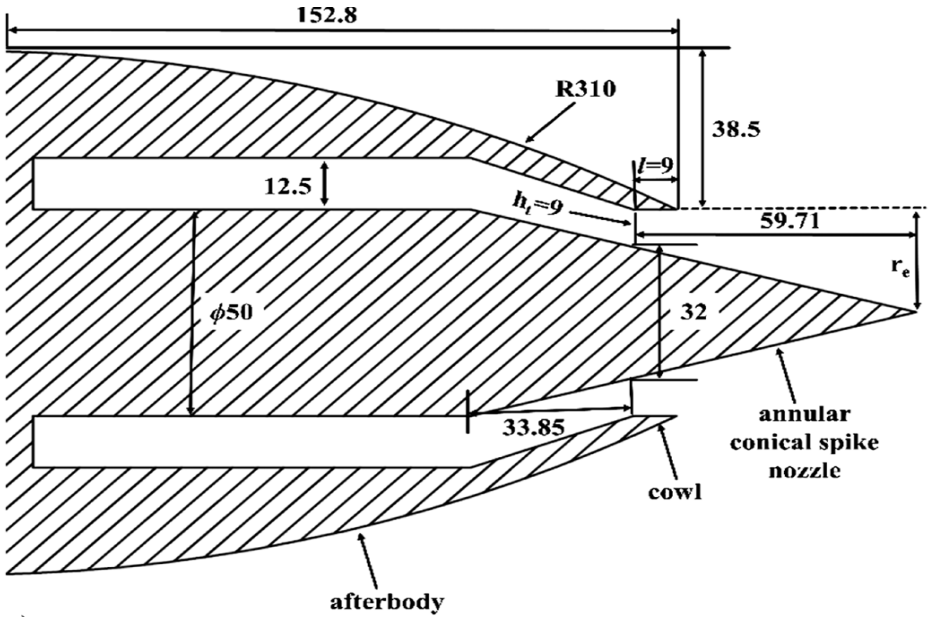


Fig 4.1 Schematic diagram of aerospike nozzle (all dimension in millimeters)

Fig 4.1 shows the computational domain used for analysis and it varied from 0 to 90 D (D is the exit nozzle diameter) horizonatally to 10 D vertically the afterbody extended up to 5D on the left side of the throat, and the inlet was kept at a distance of 2.5D from the throat.

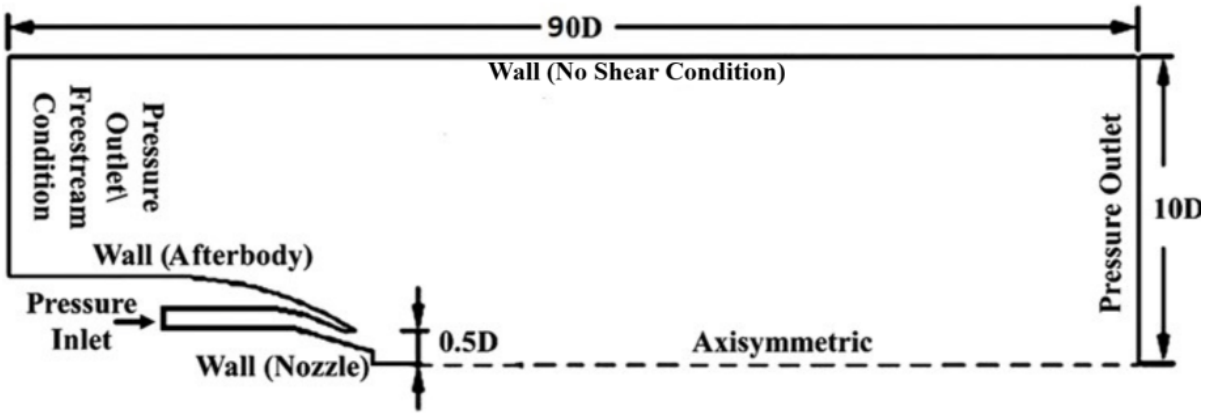


Fig 4.2 Computational Domain

4.3.1 BOUNDARY CONDITIONS

| Serial no | NPR | Pressure inlet (Pa) | Temperature Inlet (K) | Outlet -1 (Pa) | Outlet -3 (m/sec) |
|---|---|---|---|---|---|
| 1. | 2.57 | 159080 | 2382 | 0 | 545.1 |
| 2. | 3.8 | 283710 | 2382 | 0 | 545.1 |
| 3. | 6.5 | 557287 | 2382 | 0 | 545.1 |

Table 4.1

The analysis was done using a pressure-based solver and hence the jet stagnation pressure was used for the inlet boundary. Here the NPR is taken as the ratio of jet stagnation pressure $P_{oj}$ and ambient pressure $P_a$. the jet stagnation pressure was changed to vary the NPR. Freestream inflow conditions at Mach number 1.57 were used for the freestream boundary. No slip stationary wall conditions and a wall temperature of 300 K were applied to the nozzle and the rest of the body.

4.3.2 COMPUTATIONAL GRID

| Serial no | cells | Mass flow rate at nozzle exit (kg/s) | Velocity at nozzle exit (m/s) | Pressure at nozzle exit ($P_a$) |
|---|---|---|---|---|
| 1 | 52502 | 0.6913683 | | 46636.90 |
| 2 | 75860 | 0.6896836 | | 43800.45 |
| 3 | 105677 | 0.686723 | | 50368.30 |
| 4 | 140658 | | | |

Table 4.2

A 2-dimensional axisymmetric model and grid were generated using the commercial software ANSYS ICEM computational fluid dynamics (CFD). Table 1.51 shows the results of the grid independence study in which grides with different sizes were used to ensure the grid independence of the solution Grid independence tests were done by taking into consideration the effects of the computational domain used and the stretching factor to control the grid intensity near the wall. The grid was made fine near the wall region to resolve the viscosity-affected region, and y+ for the wall adjacent cell was made less than 1. The grid independence study was conducted on the truncated aerospike nozzles to reduce the influence of the grid on the computational result. The flow structure, wall pressure, mass flow rate at the exit, velocity at the exit, and pressure at the exit were compared to come to a conclusion for choosing the computational grid. From the study it is concluded that the mesh with 140658 elements shows negligible changes in mass flow rate, velocity, and pressure at the exit and any further increase in the mesh elements doesn't bring any significant change in the accuracy more over it will increase the time required for computation. The results indicate the grid independence of the solution. Convergence was judged by monitoring the inlet and outlet mass flowrates and the residuals or the time rate of change of the conserved variables in each equation, which were set below$10^{-3}$. The mesh was coarser for the far-field case which helped reduce the computational time. A domain independence study was also performed in the analysis, such that the extent of the domain did not affect the result.

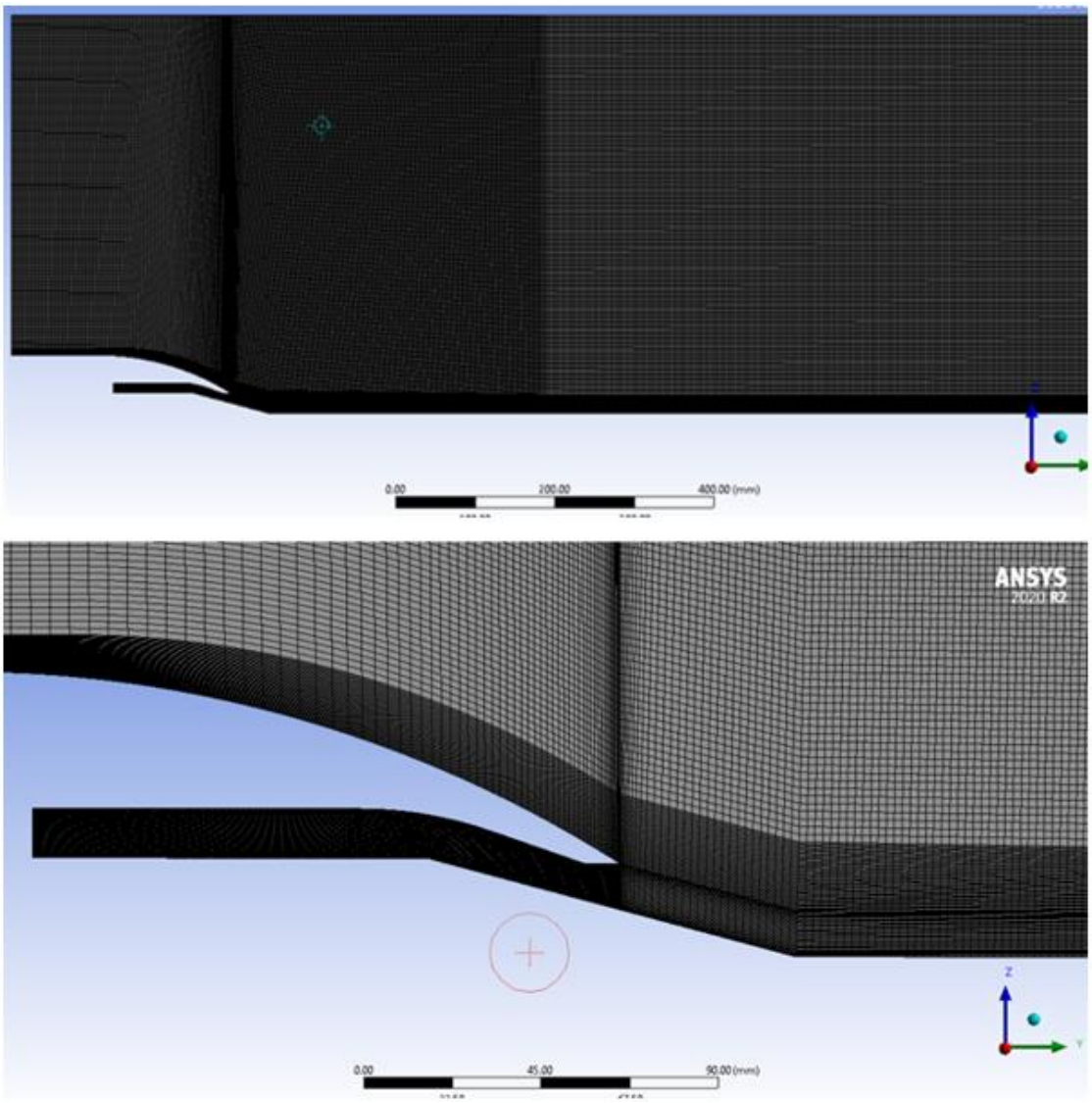


Fig 4.3 Different views of the computational grid

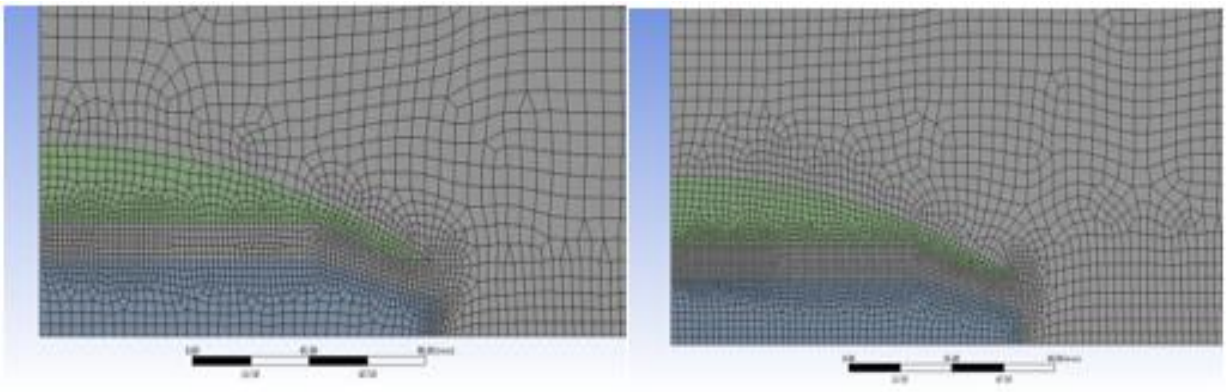

a) Elements= 52502

b) Elements= 75802

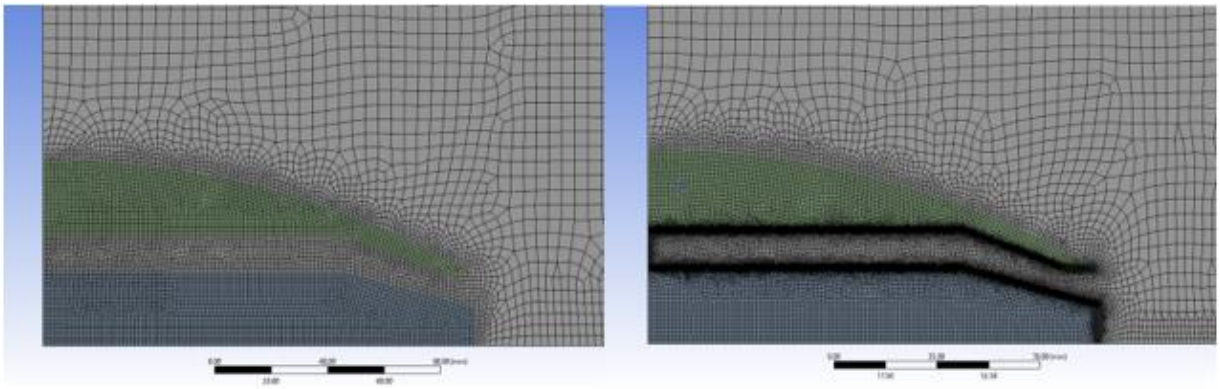

c) Elements= 105677 d) Elements= 140658

Fig 4.4 Computational Grid with number of grid elements as: a)52502, b)75802, c)105677 and d)140658

### 4.4 FLOW SOLVER

A pressure-based coupled double-precision solver was used as the baseline solver. A pressure-based coupled solver was chosen to obtain an accurate and fast converging solution. The analysis was performed under steady-state conditions. Least-squares cell based spatial discretization in which the solution was assumed to vary linearly was used. Convective terms were solved using second-order upwind interpolation scheme. The Courant number was initially kept at 10 and gradually increased as the solution progressed and was varied up to a maximum value of 20. Full multigrid initialization was performed to obtain the initial solution, and the reference values were provided from the inlet boundary.

# CHAPTER 5: RESULTS & DISCUSSIONS

## 5.1 EFFECT OF MACH NUMBER

In all the contours obtained for NPRs 2.57,3.8 and 6.5, oblique shock waves were observed to be originating near the end of the curved surface of the cowl and reflecting from the zero shear wall at the top and near the axis, throughout the entire fluid domain. It was also found that the intensity of these waves was decreasing from left to right.

Two types of shock reflections were observed- regular reflection at zero shear stress wall and Mach reflection at the axis. Mach reflection consists of three shock waves. The incident and reflected shock waves meet at a point called the triple point. From the triple point, a third shock wave extends downwards till the axis, which is the reflecting surface in our case and is called Mach stem. A drop in Mach number is observed across each Mach stem, and subsequently, there is an increase in Mach number after the decline. The change in Mach number at each Mach stem was also found to be decreasing. This variation in Mach number occurs throughout the domain at regular intervals.

This particular shock pattern may be formed because of the position of the zero-shear wall from the axis, and the pattern may change as the domain is extended upwards.

Mach number over the surface of the cowl is larger than the Mach number at nozzle exit for NPRs 2.57 and 3.8 due to the lower temperature of ambient freestream. Mach number is a function of the temperature of a fluid medium. But for the case of NPR=6.5, the higher Mach number was found to be at the exit of the nozzle. Due to the increased flow velocity at the nozzle exit, the inlet pressure is higher for the prescribed NPR. The effect of increased flow velocity dominates the impact of increased temperature, unlike for the other NPRs.

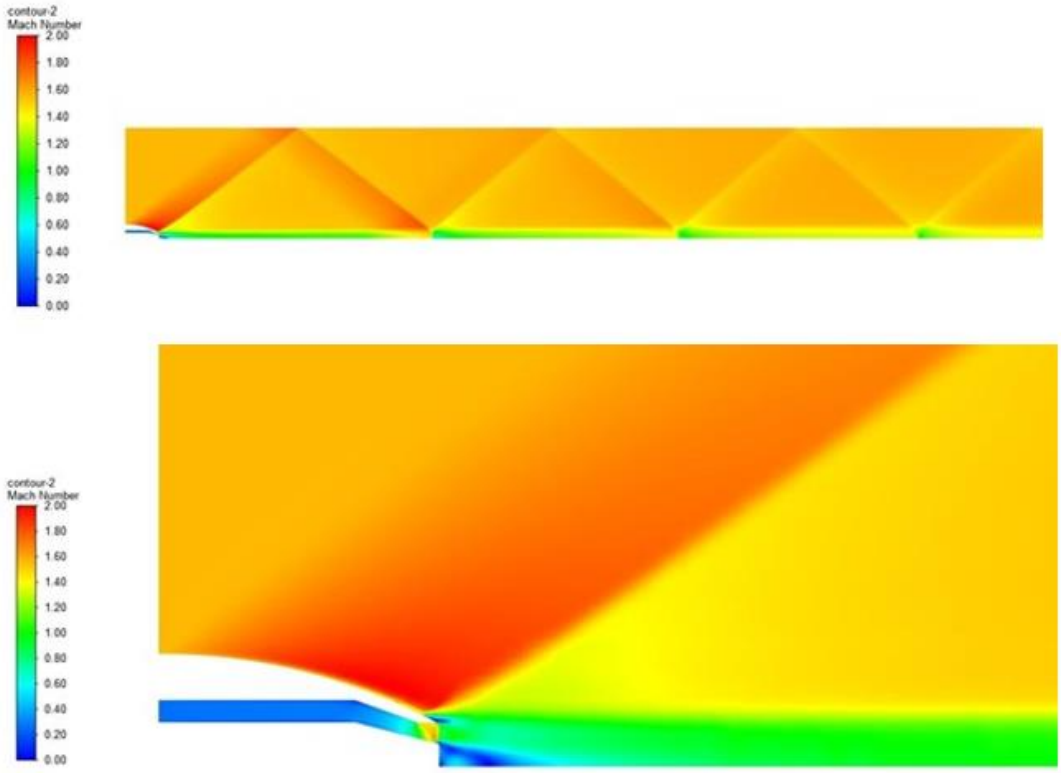


Fig 5.1 Mach number contours at NPR 2.57

A maximum Mach number value of 2 was observed at the outer surface of the cowl towards the cowl tip. This value was later found to change as NPR increases. The extent of higher Mach values over the cowl tip was noticed to be decreasing with increasing NPR.

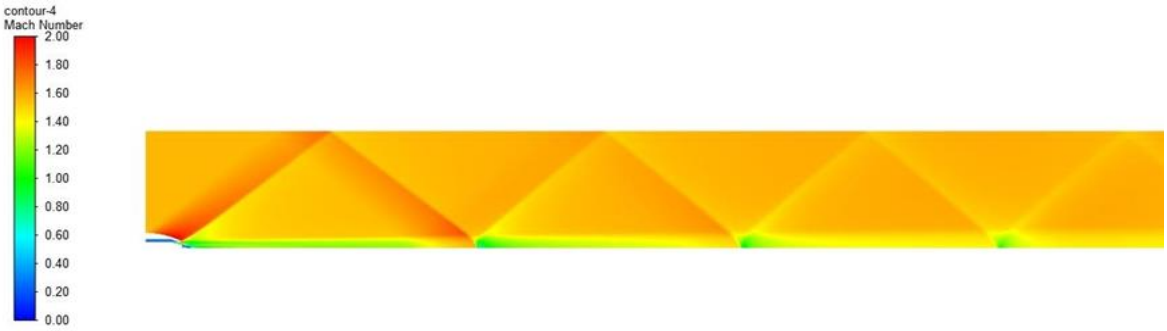

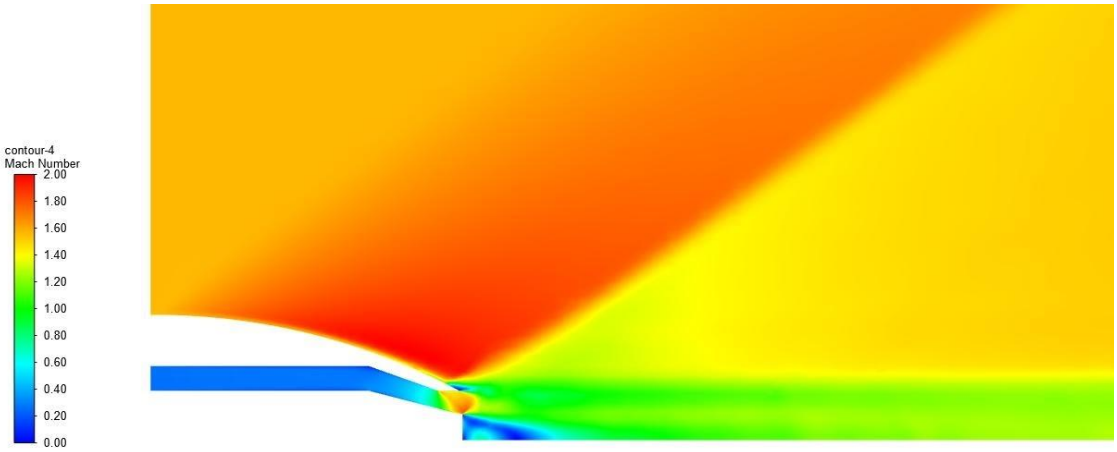


Fig 5.2 Mach number contours at NPR 3.8

For this case also a maximum Mach number value of 2 was observed at the cowl tip.

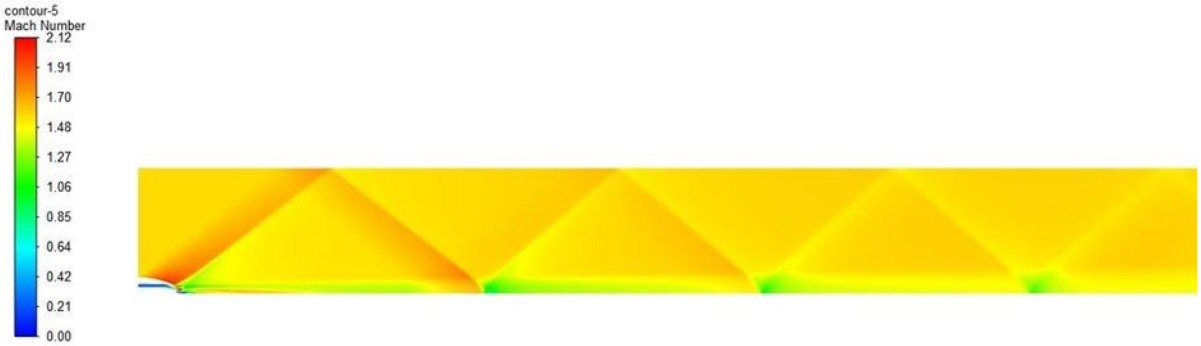


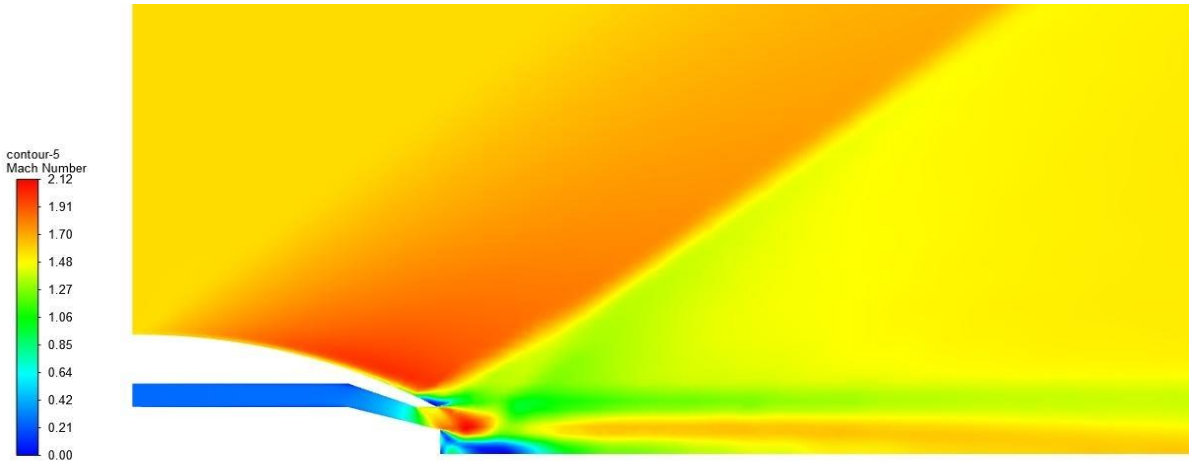


Fig 5.3 Mach number contours at NPR 6.5

Similar to the above cases a maximum Mach value of 2.119 was obtained at the nozzle exit and at the cowl surface as observed in the above cases.

## 5.2 EFFECT OF ABSOLUTE PRESSURE

Oblique shock waves can be observed in all the absolute pressure contours obtained for NPRs 2.57, 3.8, and 6.5. As there is an acceleration of fluid over the curved surface of the cowl, minimum pressure values were obtained in regions that showed maximum Mach number values. The local ambient pressure values were observed to be changing with various NPRs. From the contours obtained, it is evident that absolute pressure decreases as gas flows from the inlet to exit; consequently, the velocity of flow increases which is clearly due to the expansion of hot gases. The pattern of absolute pressure variation throughout the fluid domain is similar to that observed in Mach number contour. But absolute pressure is lower in regions where Mach number is high.

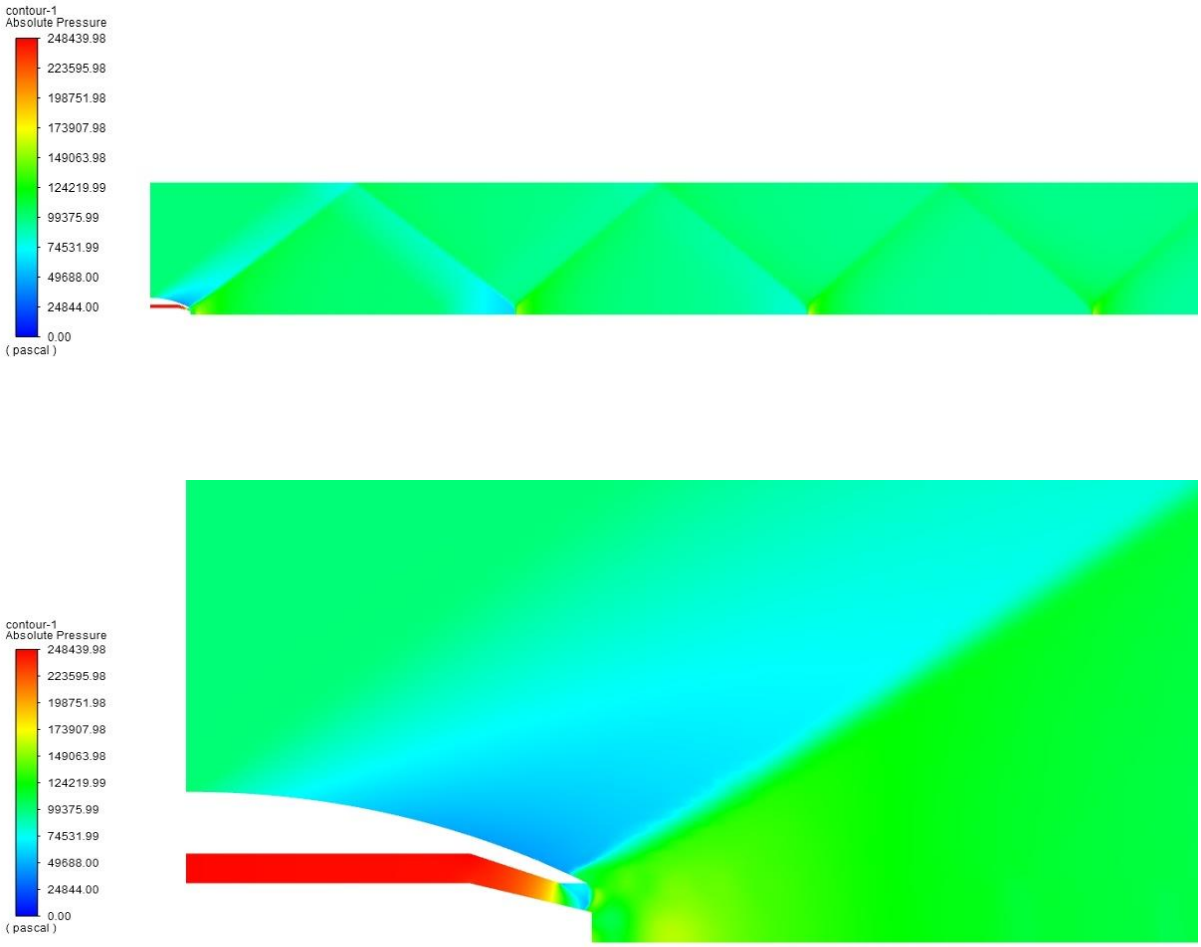


Fig 5.4 Absolute pressure contours at NPR =2.57

A low-pressure value of -54649.17 Pa was obtained at the region just above the outer surface of the cowl. A pressure value of around 46233.09 Pa was observed at areas near the nozzle exit and subsequently at points of Mach reflection. The maximum pressure value obtained here was 147115 Pa.

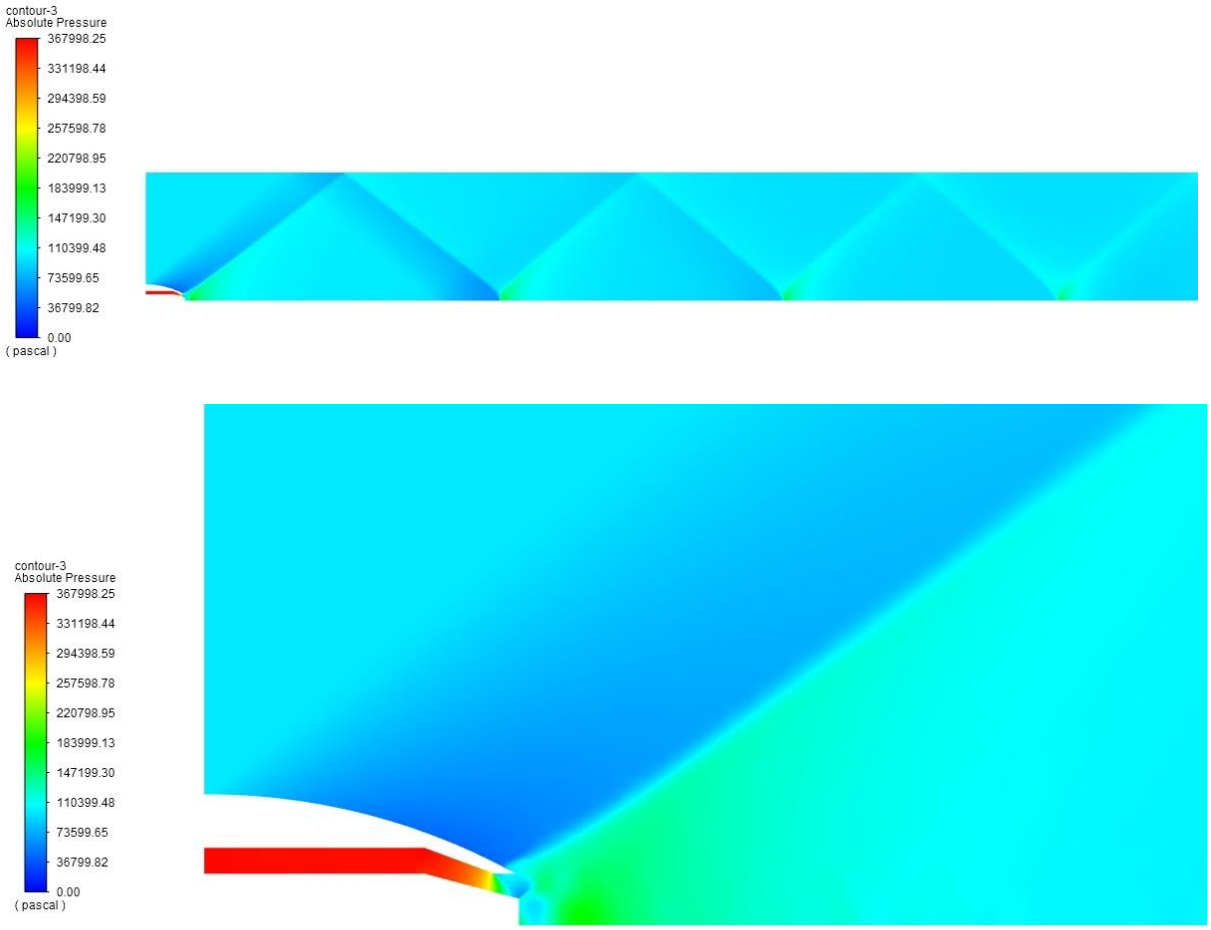


Fig 5.5 Absolute pressure contours at NPR =3.8

Minimum pressure values were obtained at the region above the cowl. The absolute pressure decreased to -54768.54 Pa from that of the value obtained for NPR 2.57. The maximum pressure value here was 266673.3 Pa.


Fig 5.6 Absolute pressure contours at NPR =6.5

The pressure value obtained near the nozzle exit is now below 120250 Pa. Minimum pressure values of 55088.41 Pa and maximum value of 529386.7 Pa, was obtained here.

## 5.3 EFFECT OF VELOCITY

Maximum velocity value changes can be observed for NPRs 2.57, 3.8 and 6.5. A flow constriction was observed near the throat, which may be formed due to the combined effects of expansion phenomenon (occurring past the throat) and freestream effects (defined by freestream Mach number 1.57). Its formation can also be linked with the phenomenon of Mach disks, generally found in conventional nozzles, that are formed through a repeating and decaying series of shocks and expansions caused by the difference between the exit pressure around the jet and the atmospheric pressure. The existence of the recirculation zone can be confirmed in all cases at the base of the spike and near the cowl lip.

The velocity of fluid over the outer surface of the cowl can be observed to be increasing till the occurrence of the shock. This increase in velocity may be due to the Coanda effect. Coanda effect is the phenomenon in which a jet flow attaches itself to a nearby surface and remains attached even when the surface curves away from the initial jet direction.

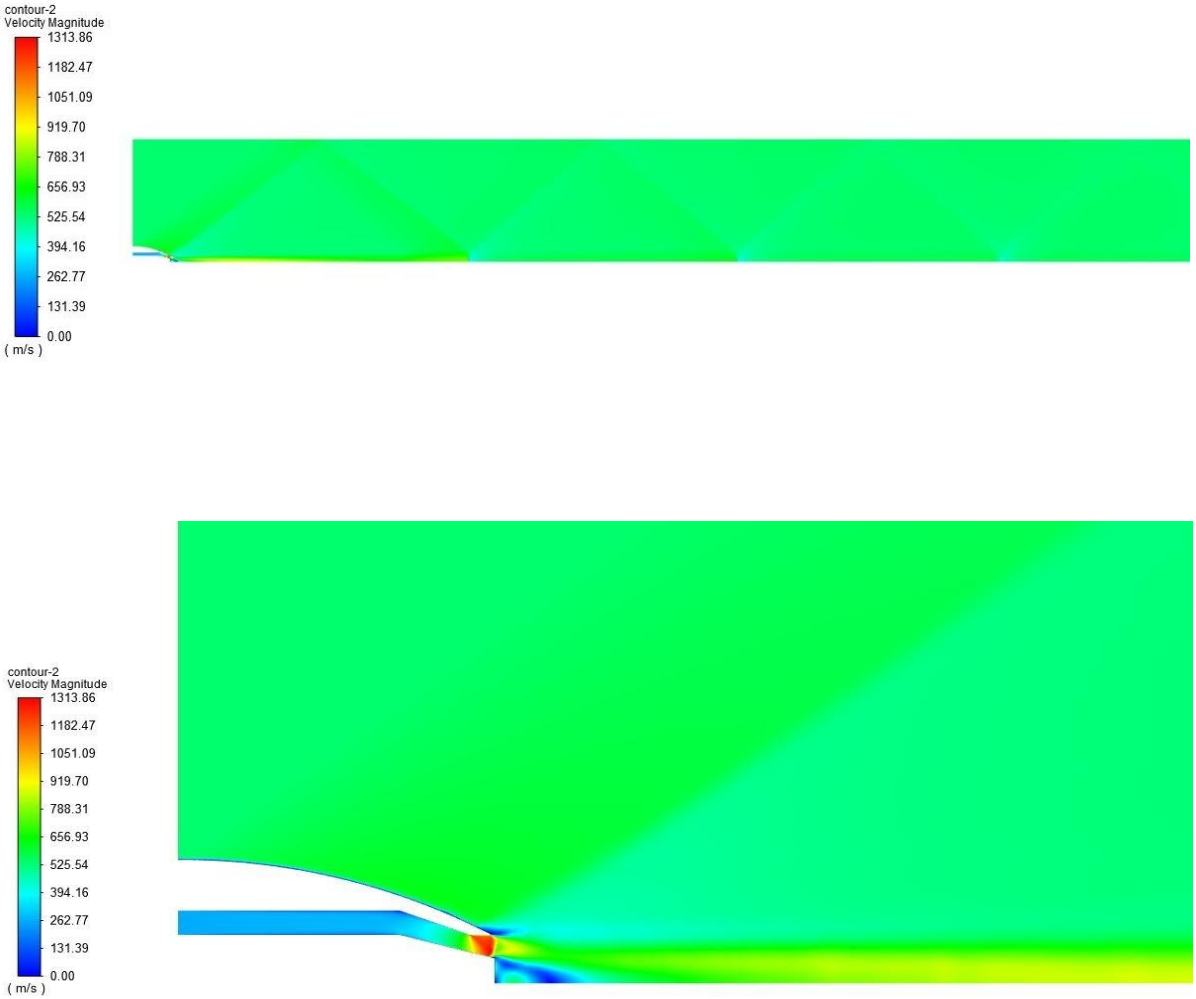


Fig 5.7 Velocity contours at NPR=2.57

The maximum velocity obtained at the throat is around 1313.857 m/s. The nozzle is now in an open wake condition.

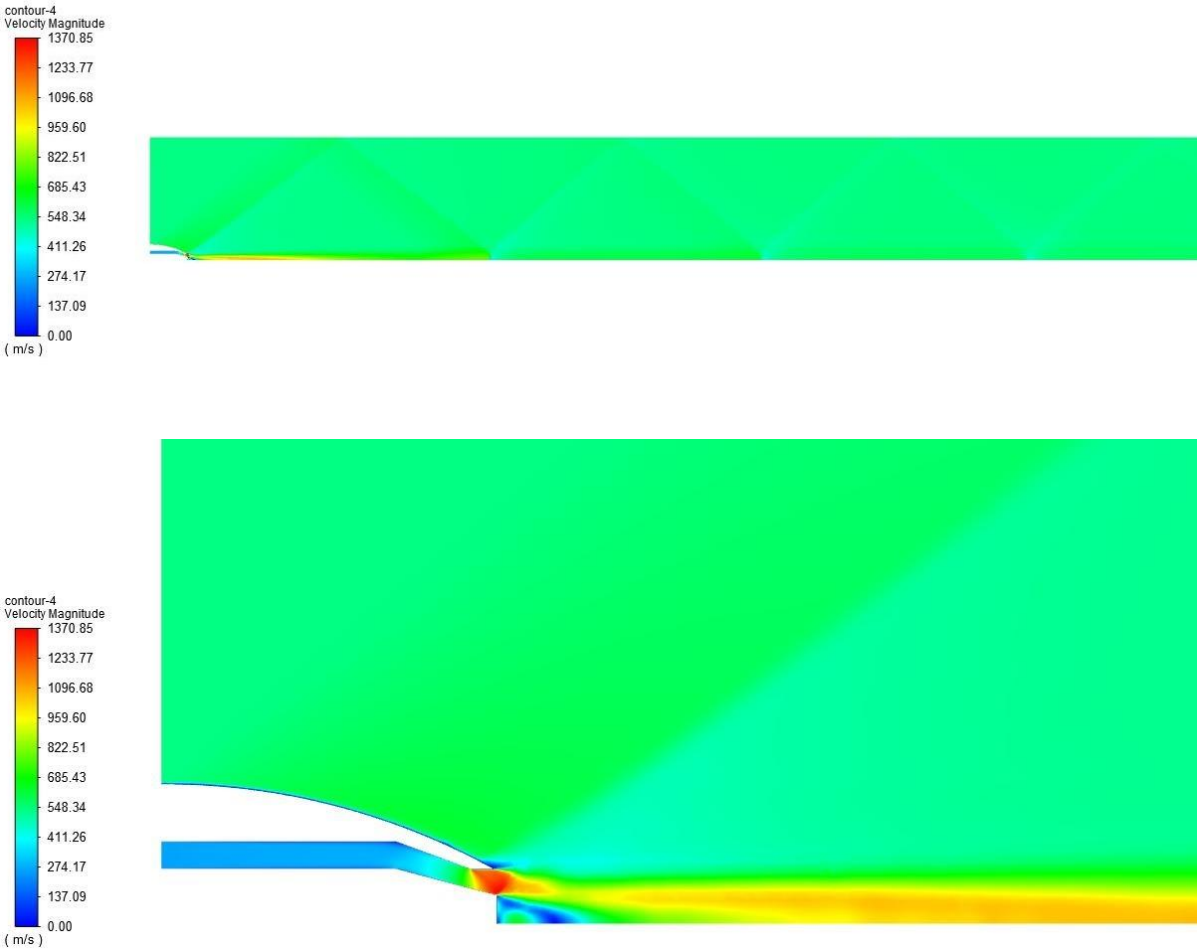


Fig 5.8 Velocity contours at NPR=3.8

The maximum velocity value at the region of the throat was now observed to be increased to approximately 1370.85 m/s.

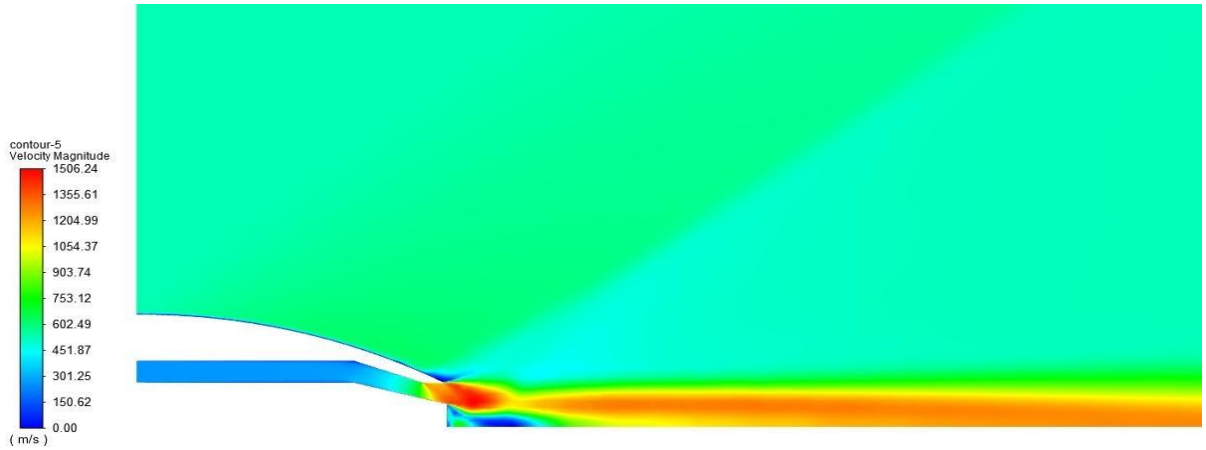


Fig 5.9 Velocity contours at NPR=6.5

The maximum velocity obtained at the region of the throat now has increased to about 1506.23 m/s.

## 5.4 EFFECT OF VELOCITY VECTORS

The direction of flow and velocity vector contour can be observed for NPRs 2.57, 3.8 and 6.5. Velocity is low at the inlet of the nozzle and increases as it reaches the region of the throat due to its constricted area. The flow then expands beyond the throat, which then influences the thrust force of a nozzle. The transition of open wake to close wake and the change in recirculation area at the base can be observed as the NPR increases.

Velocity vectors show the existence of a recirculation zone near the cowl lip. This may be due to the interaction between two fluids at different velocity conditions, i.e., the ambient freestream at Mach 1.57 and hot gases expanding through the nozzle at the nozzle exit.

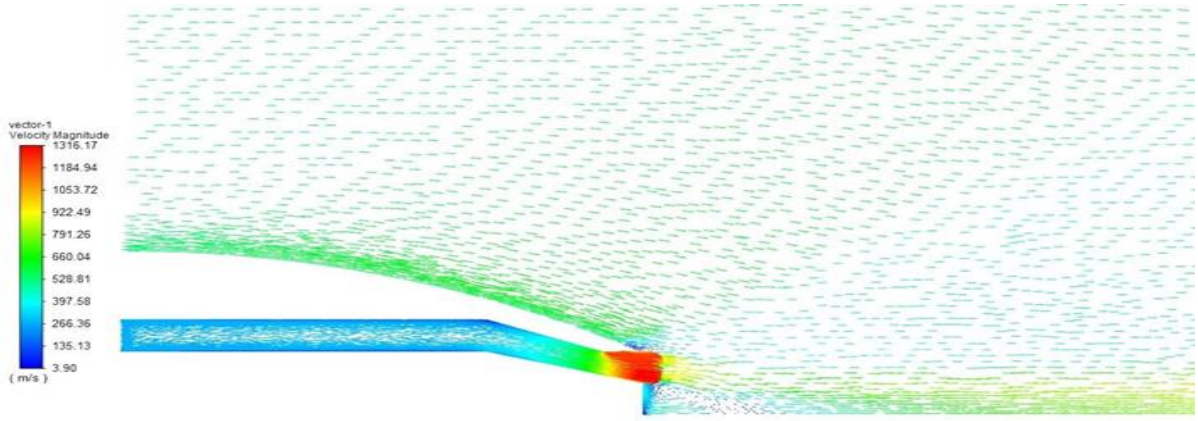


Fig 5.10 Velocity vectors at NPR=2.57

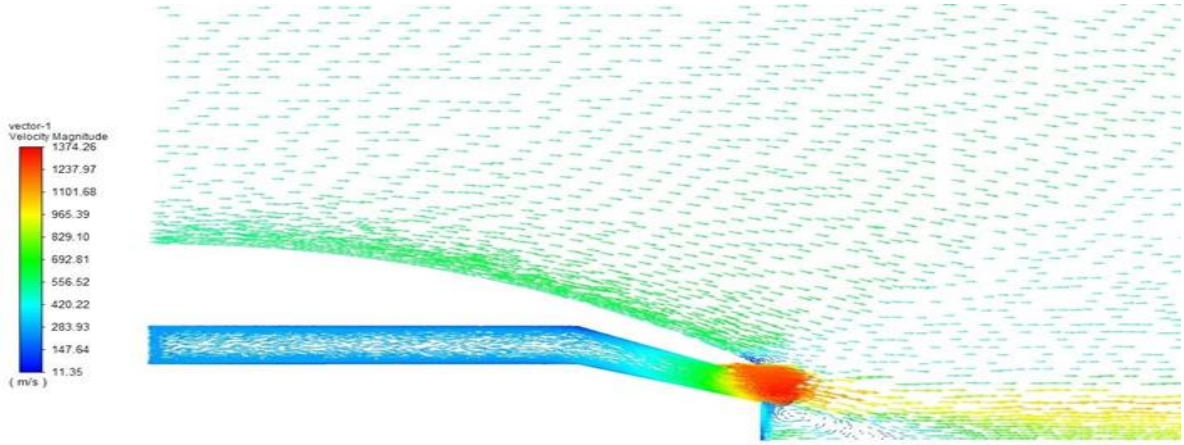


Fig 5.11 Velocity vectors at NPR=3.8

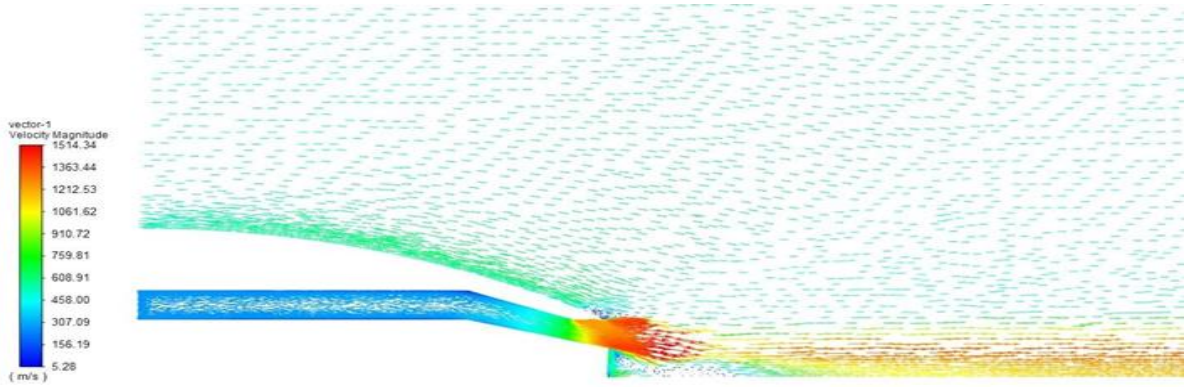


Fig 5.12 Velocity vectors at NPR=6.5

## 5.5 EFFECT OF ABSOLUTE TEMPERATURE CONTOURS BEFORE COOLING

Absolute temperature variation contours obtained without cooling effects can be observed for NPRs 2.57, 3.8 and 6.5. Adiabatic flame temperature of 2382 K was considered. Heat transfer and temperature effects were considered for a fluid domain of length 4.5m. The spike material, Ti6Al4V, has a melting point range of 1878-1923 K. Convective heat transfer phenomenon can be observed on the surface of the cowl as it interacts with the ambient conditions.

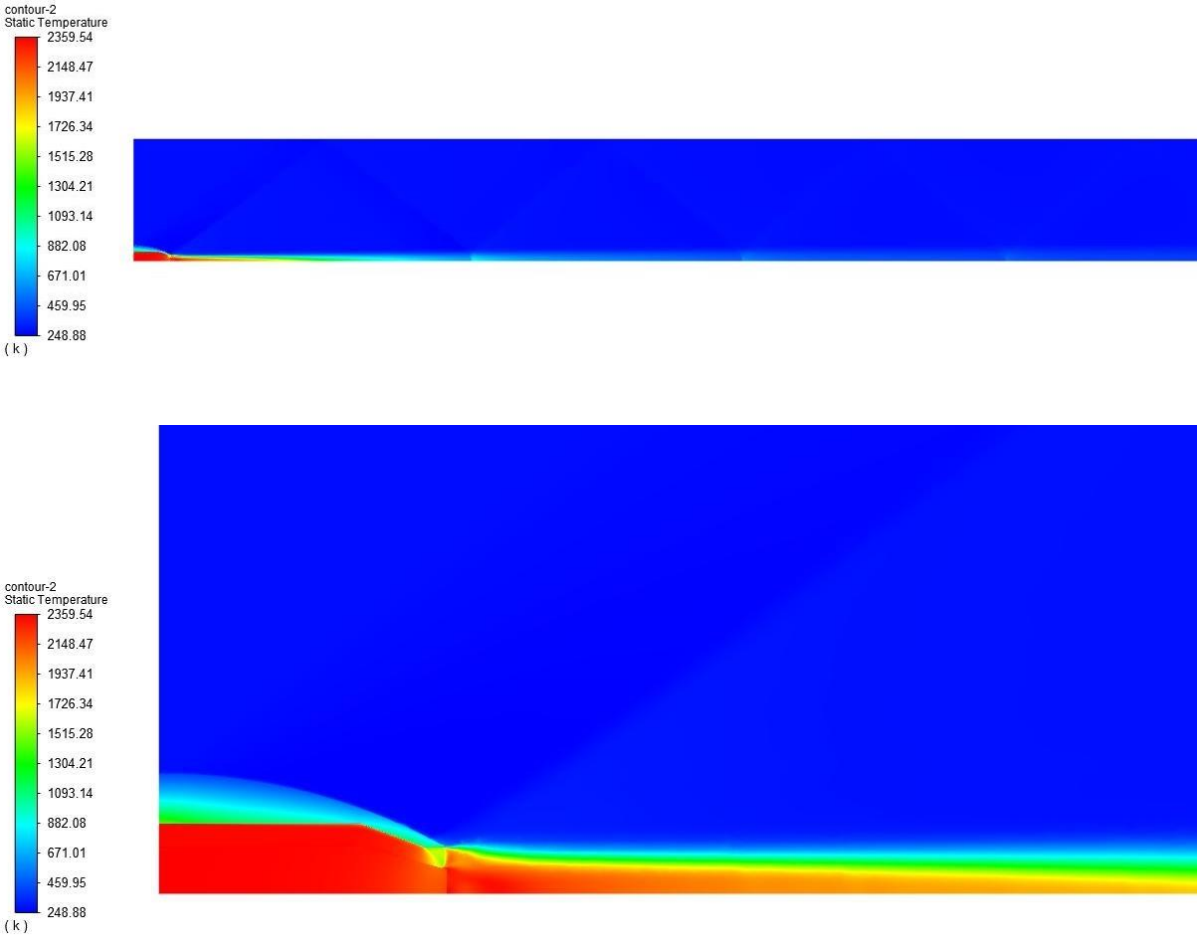


Fig 5.13 Absolute temperature contour at NPR=2.57

Compared to the spike, the cowl surface has a low temperature because of convection, as it transfers some amount of heat to the surrounding. A high temperature of about 2359.54 K is seen on the spike. Low temperatures around 1304.21 K can be seen on the interior of the cowl.

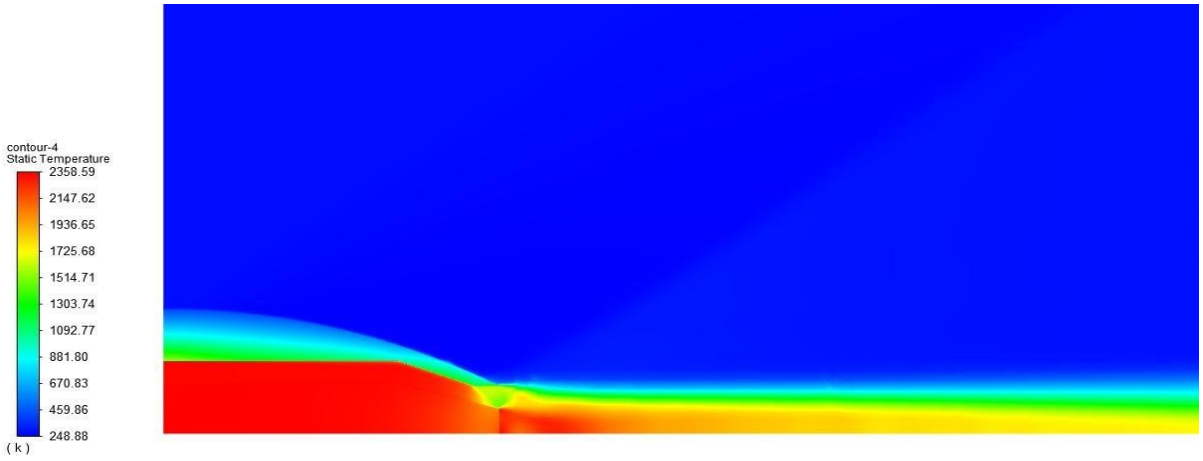


Fig 5.14 Absolute temperature contour at NPR=3.8

The high temperature obtained at the spike was around 2358.59 K. The temperature was also increasing at the interior of the cowl, which is around 1303.74 K.

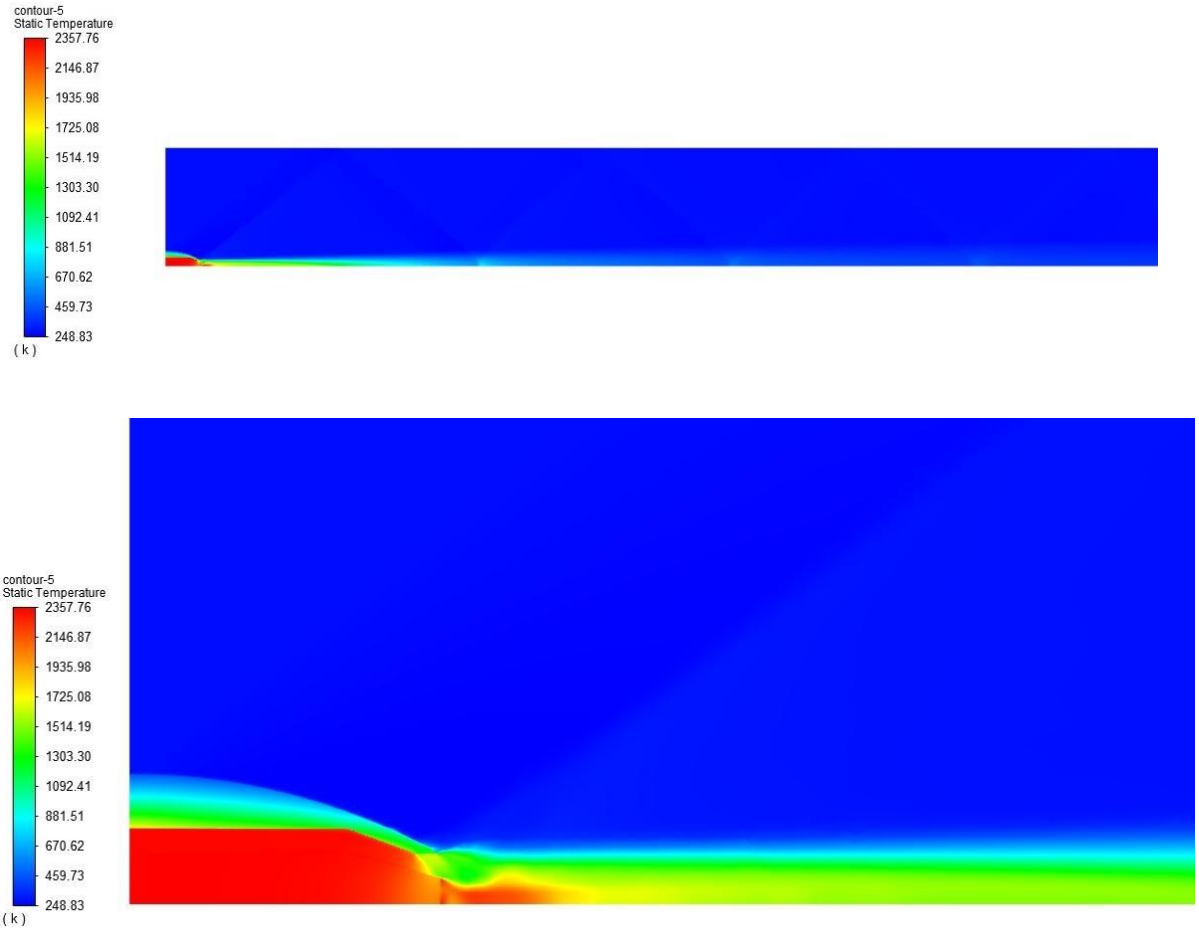


Fig 5.15 Absolute temperature contour at NPR=6.5

The temperature at the spike obtained here is 2357.76 K, which is way above the melting point of the spike material. Hence it is necessary to provide cooling at the outer surface of the spike and inner surface of the cowl to reduce the temperature to a value within the desirable limit for the safe operation of the nozzle.

## 5.6 EFFECT OF ABSOLUTE TEMPERATURE CONTOURS AFTER COOLING

Absolute temperature contours obtained after cooling effects were observed for NPR 2.57, 3.8 and 6.5. Since the temperature obtained without cooling was well above that of the melting point temperature of the spike material, it was necessary to provide cooling to the spike. Comparatively, the inner surface of the cowl (top wall) was given a heat generation value of -14e7 W/m3, which is lower than that given to the outer surface of the spike (bottom wall), -24e7 W/m3, because of the convective heat transfer found around the surface of the cowl as it interacts with the surroundings.

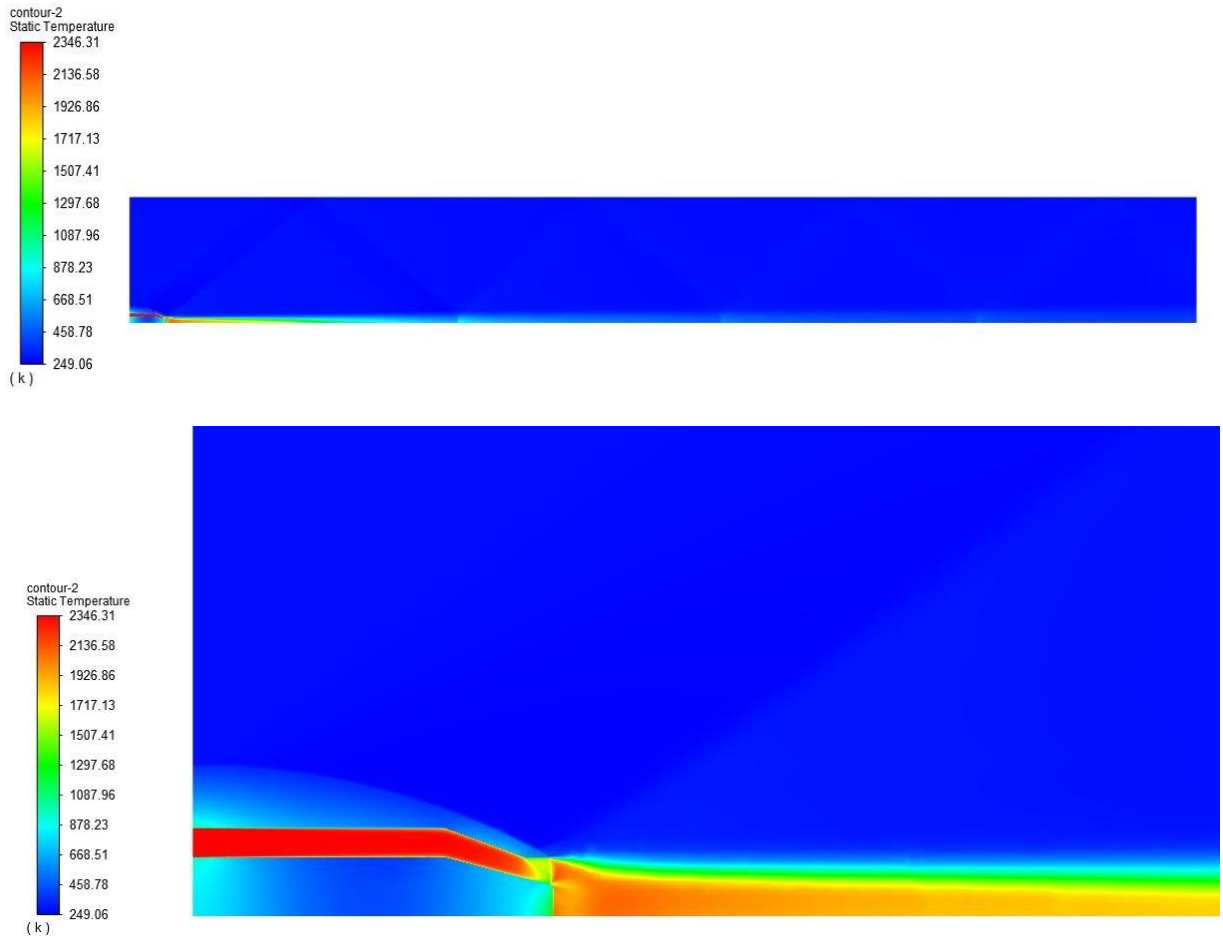


Fig 5.16 Absolute temperature contour at NPR=2.57

The spike temperature here is around 878.23 K, which is well below the melting point value.

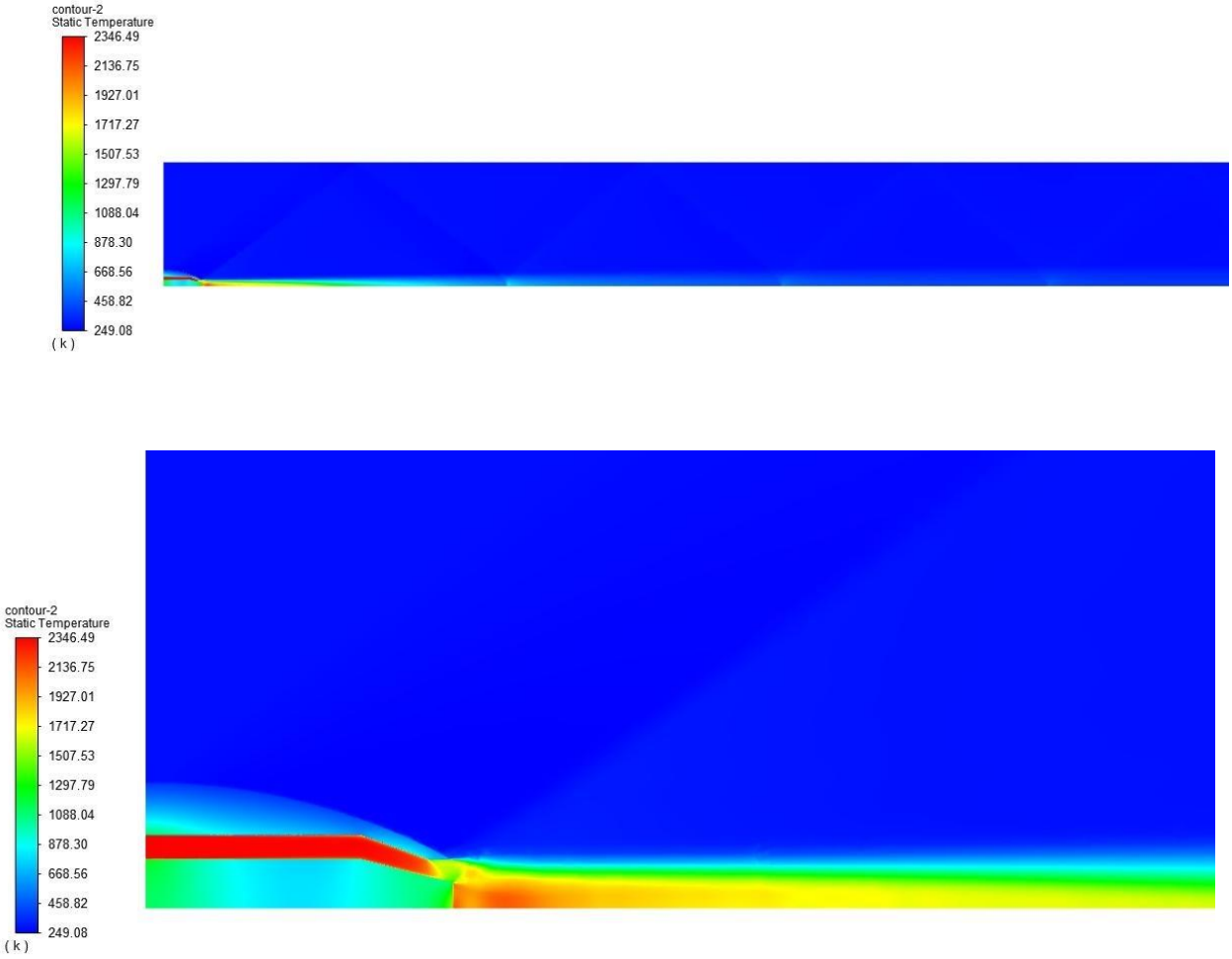


Fig 5.17 Absolute temperature contour at NPR=3.8

The temperature of the spike here is also well within the safety limit. A slight temperature increase of about 1297.79 K can be observed at the inlet and base of the spike.

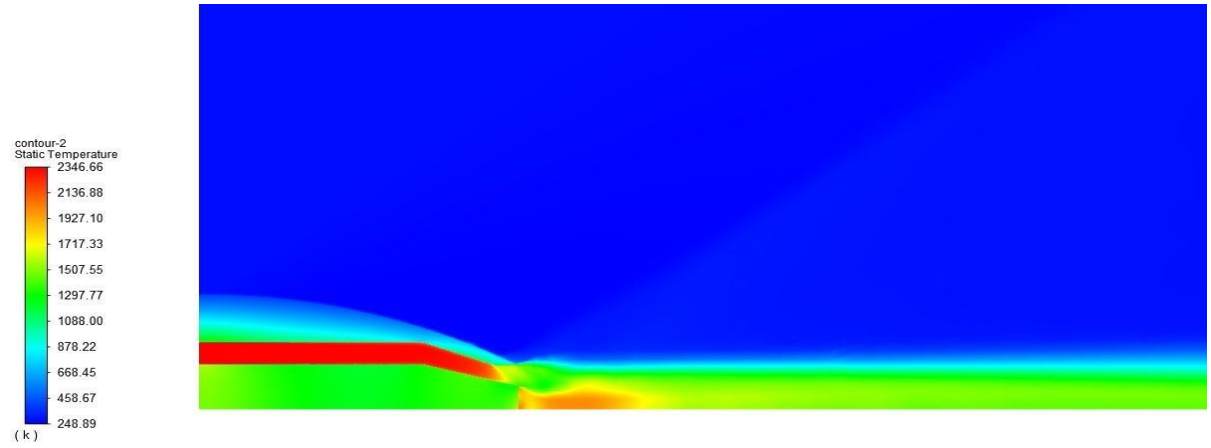


Fig 5.18 Absolute temperature contour at NPR=6.5

The temperature here is around 1297.77 K. A slight temperature change can be observed at the interior of the cowl here.

## 5.7 GRAPHS

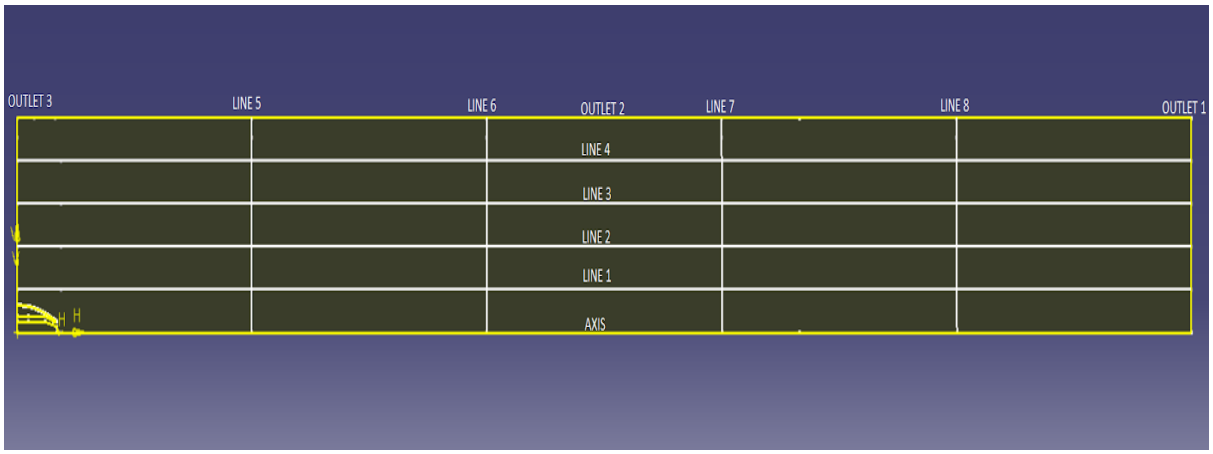


Fig.5.19 Domain divisions

To understand the variation of properties throughout the fluid domain, it was divided into five sections vertically and horizontally, as shown in the figure.

5.7.1 EFFECT OF EXHAUST TEMPERATURE ALONG THE AXIS

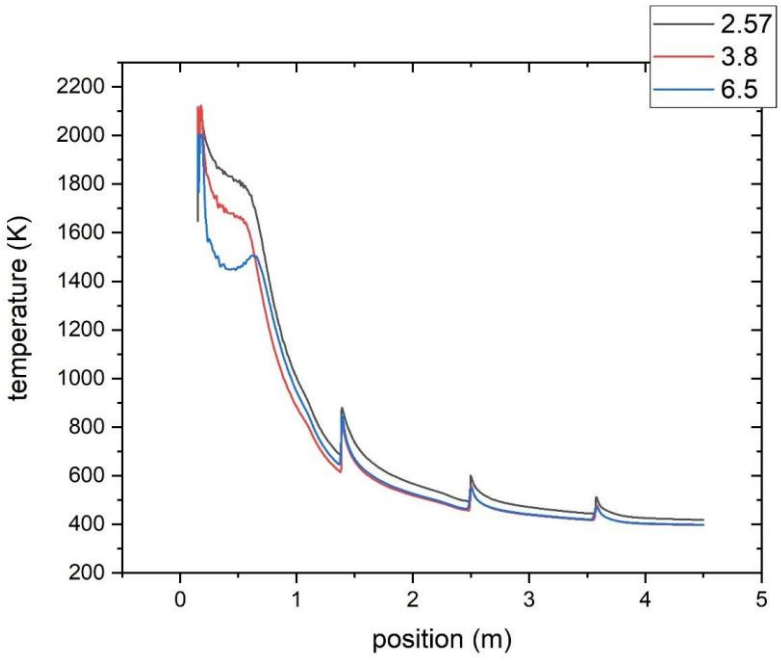


Fig 5.20 Temperature distribution along the axis of domain

Temperature vs position along the axis is shown in the figure. In the beginning, the temperature values were increasing for the three NPRs due to the presence of a recirculation zone at the base. After that, as the expansion occurred, the values started to decrease and gradually approached near ambient temperatures. In between this gradual change, a slight increase in the temperature values was noticed at regular intervals of approximately 1.1m. The positions where these peaks were found are at the places where Mach reflections occurred. It was noted that at a distance of 3.75m along the axis, the temperature of the fluid reaches a value of 400K, which is a safe limit of temperature.

5.7.2 EFFECT OF MACH NUMBER ALONG THE HORIZONTAL DIVISIONS IN DOMAIN

From Mach number vs position plots, we can observe that the Mach number inside the triangle, between an incident and reflected shock is close to the applied freestream Mach number value of 1.57. Also, variation in Mach number is due to the formation of shock.

It can also be noted that the peak value of Mach number before the formation of an incident shock is higher than the subsequent shock formed after reflecting from a surface. Therefore, the peak value of Mach number is seen to be decreasing from shock to shock.

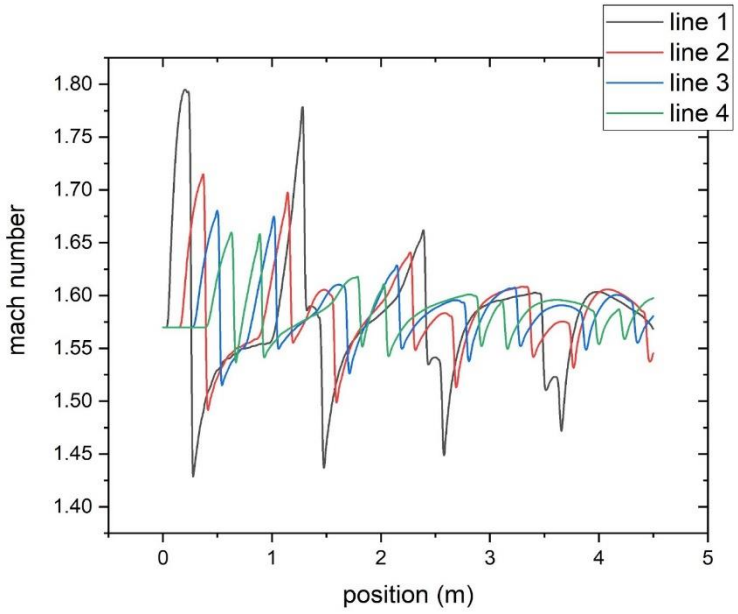


Fig 5.21 Mach number distribution along the horizontal lines at different NPRs

### 5.7.3 EFFECT OF EXHAUST TEMPERATURE ALONG THE VERTICAL DIVISIONS IN DOMAIN

The variation of temperature along directions perpendicular to the axis can be observed in the figures. Five vertical lines equidistant to each other were chosen to study the variation as shown in Fig 5.19.

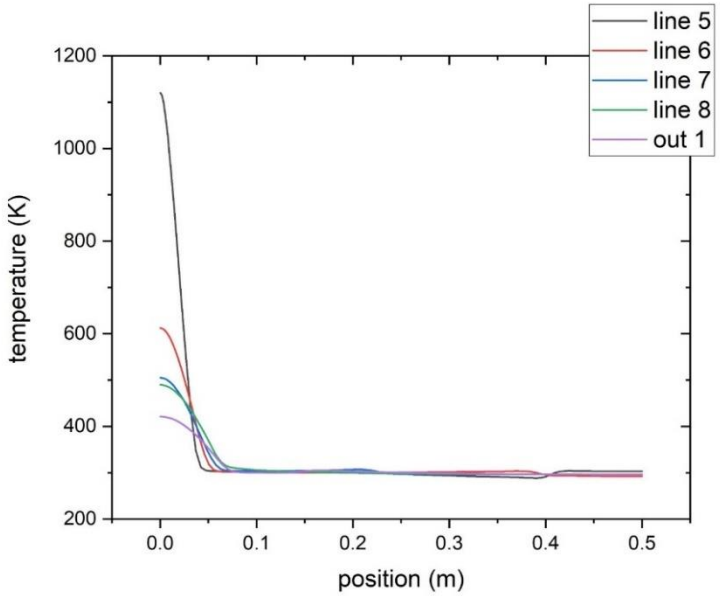


Fig 5.22 Temperature distributions along the vertical lines for NPR=2.57

Here initially, the maximum temperature is for line 5 since it is closer to the nozzle exit. It corresponds to a temperature value of 1120.65 K, which is near to the exhaust. For the other lines, as the distance from their initial points from the nozzle exit increases, the initial temperature decreases. As we move away from the axis along these lines, the temperature values drop to ambient temperature. For all the lines, the temperature reaches the ambient condition at approximately 0.1m in this case.

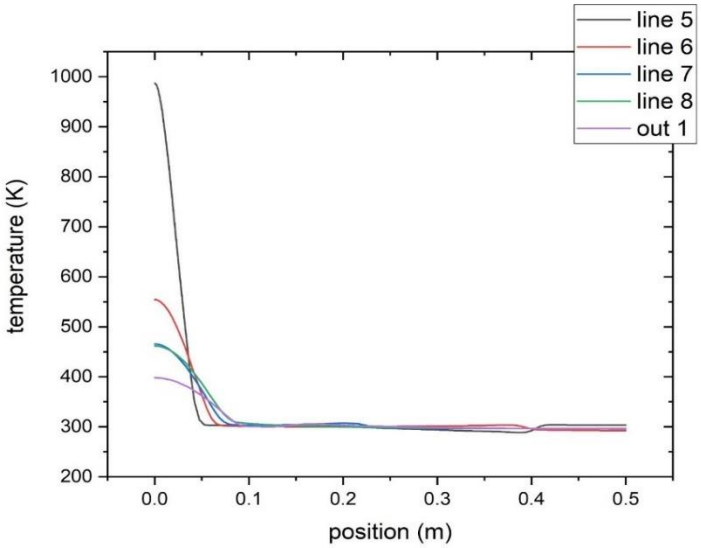


Fig 5.23 Temperature distributions along the vertical lines at NPR=3.8

A similar pattern obtained for the above case of NPR=2.57 is observed here also. The initial temperature for line 5 was found to be 966.24K. Also, all the lines reach the ambient temperature at a distance of approximately 0.1m away from the axis.

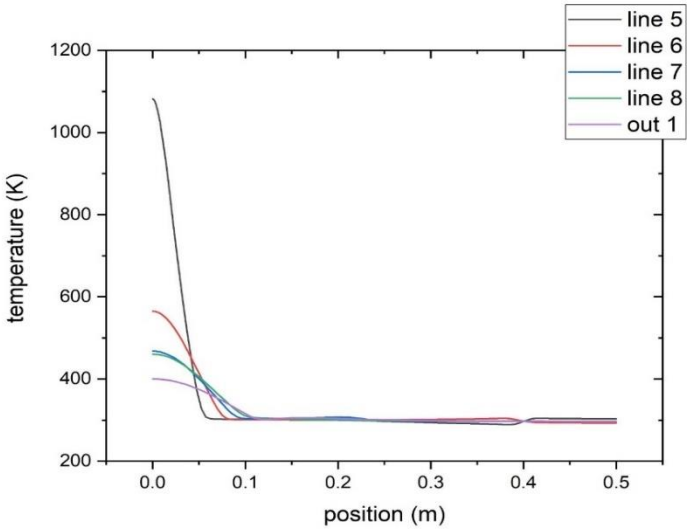


Fig 5.24 Temperature distributions along the vertical lines at NPR=6.5

The pattern observed in this case is identical to that of others. The initial temperature of line 5 is 1081.91K. The ambient temperature is attained at a distance of 0.12m away from the axis for all the lines.

### 5.7.4 TEMPERATURE VARIATIONS ON THE SURFACES AFTER COOLING AT DIFFERENT NPRs

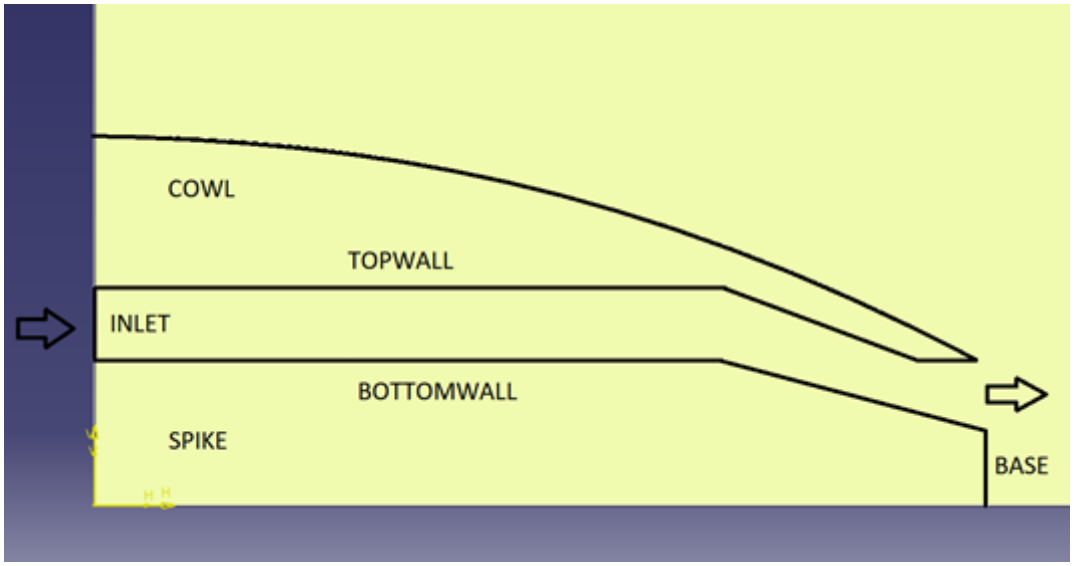


Fig 5.25 Schematic representation of the modelled aerospike

#### 5.7.4.1 EFFECTS OF EXHAUST TEMPERATURE ON SPIKE

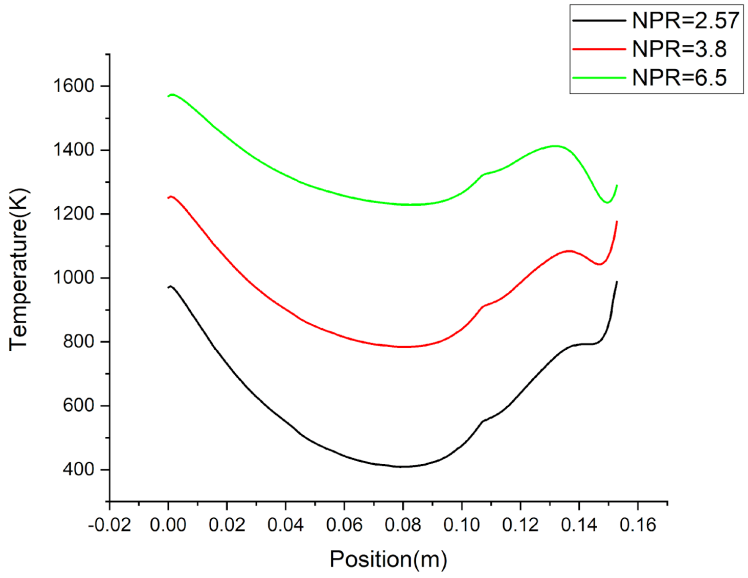


Fig 5.26 Temperature distribution along the outer surface of the spike for various NPR

Variation concerning temperature along the outer surface of the spike (bottom wall) for NPRs 2.57, 3.8, and 6.5 was obtained, as shown above. The initial portion of the graph indicates the flow of incoming hot fluid. The gradual decrease in temperature is due to the heat transfer of the hot fluid with the coolant. The increase in temperature after the dip is observed to be due to the subsequent change in geometry, tapered towards the end of the spike. This change reduces the cooling channel volume, decreasing the cooling effect at that region and increasing the temperature. Expansion of fluid past the throat can be seen as a decrease in temperature found towards the end of the plotline. The cooling range varies according to the changes in NPR, with the heat generation value constant for all cases. The lowest(dip) temperature difference between the NPRs 2.57 and 3.8 is 374.792 K, and NPRs 3.8 and 6.5 is 445.458 K.

The inlet, lowest, and exit temperature attained for the different NPRs are as follows:

i) At 2.57

Inlet - 970.145 K, Lowest (dip) - 409.35 K, Exit - 987.66 K

ii) At 3.8

Inlet - 1250.87 K, Lowest (dip) - 784.142 K, Exit - 1176.56 K

iii) At 6.5

Inlet - 1568.96 K, Lowest (dip) - 1229.6 K, Exit - 1288.9 K

### 5.7.4.2 EFFECT OF EXHAUST TEMPERATURE ON COWL

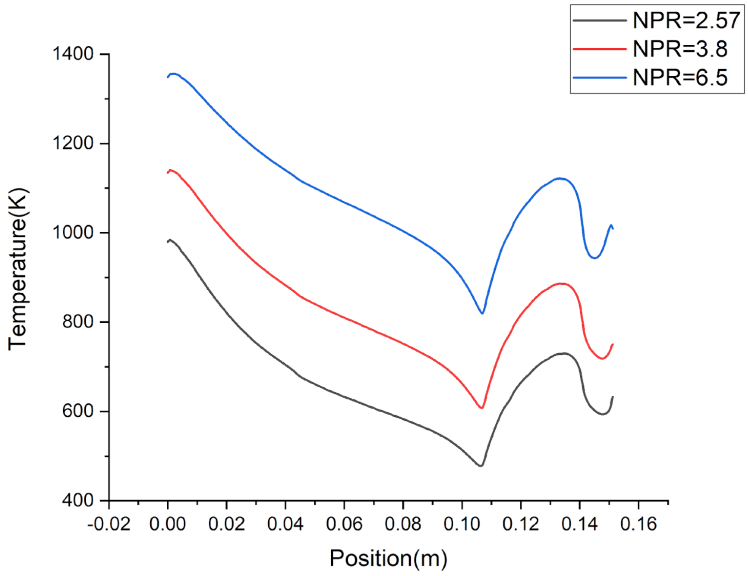


Fig 5.27 Temperature distributions along the inner surface of the cowl for various NPR

Variation of temperature along the inner surface of the cowl (top wall) for NPRs 2.57, 3.8, and 6.5 was obtained, as shown above. The initial portion of the graph indicates the flow of incoming hot fluid. A sudden decrease in temperature is seen here compared to the gradual trend found in the spike's outer surface. This decrease indicates the heat transfer of the hot fluid with the coolant and atmosphere(convection). After the dip, the reduced volume of the cowl region is why a sharp increasing trend is found for all the cases. Expansion of fluid past the throat can be seen as a decrease in temperature found towards the end of the plotline. The cooling range varies according to the changes in NPR, with the heat generation value constant for all cases. The lowest(dip) temperature difference between NPRs 2.57 and 3.8 is 129.9 K and NPRs 3.8 and 6.5 is 211.42.

The inlet, lowest, and exit temperature attained for the different NPRs are as follows:

i) At 2.57

Inlet - 981.1 K, Lowest (dip) - 478.4 K, Exit - 631.98 K

ii) At 3.8

Inlet - 1134.82 K, Lowest (dip) - 608.3 K, Exit - 750.1 K

iii) At 6.5

Inlet - 1350.38 K, Lowest (dip) - 819.72 K, Exit - 1013.42 K

# CHAPTER 6: CONCLUSION

# REFERENCES


Hagemann, G., Immich, H., Van Nguyen, T. and Dumnov, G., 1998. Advanced Rocket Nozzles. *Journal of Propulsion and Power*, 14(5), pp.620-634.

Harroun, A., Heister, S., Sardeshmukh, S. and Ruf, J., (**2019**). Effect of Aerospike Plug Nozzle Design on Rotating Detonation Engine Performance for Rocket Applications. *AIAA Scitech 2019 Forum*.

He, M., Qin, L. and Liu, Y., (**2015**). Numerical investigation of flow separation behavior in an over-expanded annular conical aerospike nozzle. *Chinese Journal of Aeronautics*, 28(4), pp.983-1002.

Nair, P., Suryan, A. and Kim, H., (**2017**). Computational study of performance characteristics for truncated conical aerospike nozzles. *Journal of Thermal Science*, 26(6), pp.483-489.

Nair, P., Suryan, A. and Kim, H., (**2019**). Study of Conical Aerospike Nozzles with Base- Bleed and Freestream Effects. *Journal of Spacecraft and Rockets*, 56(4), pp.990-1005.

Sule, W. and Mueller, T., (**1973**). Annular Truncated Plug Nozzle Flowfield and Base Pressure Characteristics. *Journal of Spacecraft and Rockets*, 10(11), pp.689-695.

Varvill, R. and Bond, A., **2003**. A Comparison of Propulsion Concepts for SSTO Reusable Launchers. *JBIS*, 56, pp.108-117.

Verma, S., (**2009**). Performance Characteristics of an Annular Conical Aerospike Nozzle with Freestream Effect. *Journal of Propulsion and Power*, 25(3), pp.783-791.

Verma, S. and Viji, M., (**2011**). Freestream effects on base pressure development of an annular plug nozzle. *Shock Waves*, 21(2), pp.163-171.